Improving Control and Functionality of Photoredox-Mediated Metal-Free Ring-Opening

Metathesis Polymerization

By

Rachel L. Tritt

A dissertation submitted in partial fulfillment of

the requirements for the degree of

Doctor of Philosophy

(Chemistry)

at the

UNIVERSITY OF WISCONSIN–MADISON

2023

Date of final oral examination: 08/04/2023

The dissertation is approved by the following members of the Final Oral Committee:
      Andrew J. Boydston, Professor, Chemistry
      Padma Gopalan, Professor, Materials Science and Engineering
      David M. Lynn, Professor, Chemical and Biological Engineering
      Jeffrey D. Martell, Assistant Professor, Chemistry

Acknowledgements

There are many people I have to thank for helping me get to where I am today, but preeminent among them is my family, namely my parents, Bob and Louise Tritt, and my sister, Sarah Tritt. They have supported me through what has seemed like an endless education and dealt with a lot of my highs and lows during that process. I would also like to thank my aunt and uncle, Susan and Steve Vogl, as well as many other extended family members, especially Trish Tritt and Brian Pritchard, for continuing to be interested in my progress.

It goes without saying that all of the teachers I have had along the way played a significant part in my being able to make it this far, but a few stand out in my mind: my middle school science teacher, Jim Flournoy; my high school English teacher, Melissa Wilcox; so many of my Lafayette Chemistry professors, including Xiadong Fan, Roxy Swails, Melissa Gordon (CBE), Chip Nataro, Ken Haug, and, of course, my undergraduate research advisor, Daniel Griffith.

I also, naturally, have many fellow graduate students and group members to thank, for problem solving and venting reasons alike; among them are Xuejin Yang, Vinnie Rigoglioso, Sean Gitter, Cody Schilling, Meg Tetzloff, Brittany Trinh, Marco Lopez, Steven Chapman, and especially Kyle Chin. I am also very grateful to my advisor, AJ Boydston, as well as to the rest of my thesis committee for their time and consideration.

Table of Contents

Abstract

Ring-opening metathesis polymerization (ROMP) involves the reaction of strained cyclic olefins to create polymers that retain the unsaturation of the initial monomer. Traditionally, this transformation has been achieved using metal alkylidene initiators, typically centered around one of three transition metals (Ru, Mo, W). While this strategy has many advantages, such as well-defined initiators, functional group stability, and microstructural control, an alternate, fully organic mechanistic strategy is possible (MF-ROMP). This method is distinct from its metal-based predecessor as it is enabled by photoredox-generated radical cationic species. As a result, it is subject to different considerations, specifically surrounding the behavior of the active chain-end. MF-ROMP also has different capabilities and possible applications due to this change in reactivity, which makes the development of this technology of great interest to us.

This dissertation will first contextualize MF-ROMP, providing background on traditional ROMP, as well as on the electrochemical and photochemical cyclobutanations that inspired the development of the metal-free, photoredox-mediated method on which this document is centered. The initial development of MF-ROMP will also be covered in this section (Chapter 1).

Next, the proposal for and discovery of the cross-metathesis method for chain transfer in MF-ROMP will be discussed, leading into preliminary work to leverage this mechanism for a fully organic system for small molecule cross-metathesis (Chapter 2).

The use of chain transfer will then continue into the development of silane-functionalized polymers and oligomers for use in fiber-reinforced composites. Future directions for these materials and methods are also included, as well as preliminary results for extending this work into surface-initiated MF-ROMP (Chapter 3).

The modulation of molar mass dispersity (Đ) is introduced next, illustrating the effect that simple changes to reaction conditions have on the progression of the polymerization. Suggestions for additional investigations based on this discovery are also included (Chapter 4).

Finally, a cursory study on the ability to use aromatic alkenes as initiators in MF-ROMP is summarized. This work is also accompanied by a reflection on current limitations and future development of the technology (Chapter 5).

Chapter 1: Background and Motivation

Ring-opening metathesis polymerization (ROMP) is a method of producing polymer chains from strained, cyclic olefins. It is distinct from most other olefin polymerizations because the final product retains the unsaturation of the original monomer. This is achieved through metathesis, a term borrowed from Greek (μετάθεσις means "to transpose"), here indicating the rearrangement of carbon—carbon double bonds. This was initially accomplished using transition metal catalysts and, in addition to ROMP, can be used for ring-opening metathesis (ROM), ring-expansion metathesis polymerization (REMP), ring-closing metathesis (RCM), acyclic diene metathesis (ADMET) polymerization, or cross-metathesis (CM).[1] These transformations are summarized in Scheme 1.1a. After the initial discovery of this capability in the 1950s, it took many years for the mechanism as we understand it today (Scheme 1.1b) to be proposed and tested, and it was not until the 1980s that well-defined catalysts were developed. Since then, the field
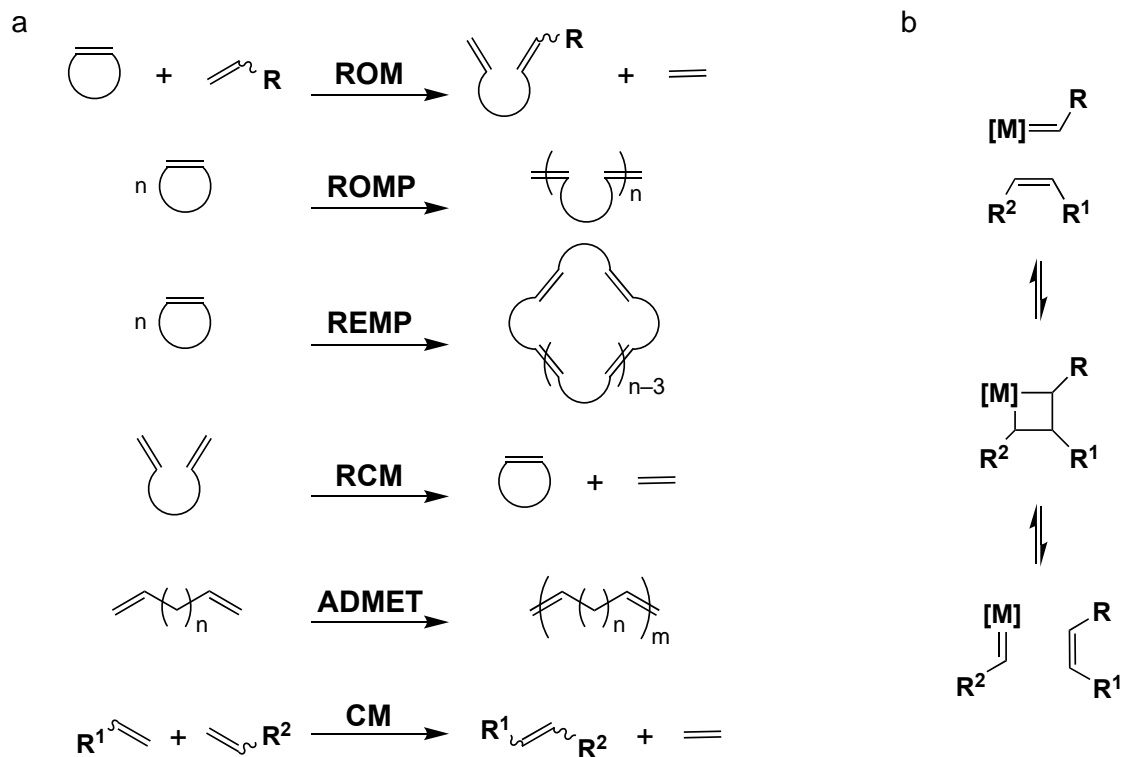
Scheme 1.1. a) Transformations achieved through olefin metathesis and b) its general, metal-based mechanism.

has grown significantly and boasts many specialized catalysts that can be used to achieve high functional group tolerance,[2-3] microstructural control,[4-5] and external control (i.e., with light, temperature).[6-8] It is noteworthy that most of these catalysts and initiators are based on a few transition metals: most commonly, ruthenium, molybdenum, and tungsten. Very recently, some groups have begun reporting on non-precious metal-based metathesis reactions (vanadium and iron).[9-12] While the development of those systems is behind those based on more precious metals, if the same level of versatility can be achieved with non-precious metals, the impact of metathesis materials will shift significantly. This is because while the metathesis method has seen commercialization in certain situations (e.g., alkenolysis-based biorefining, pharmaceutical synthesis using RCM, ROMP oligomer-based reagents and scavengers), it is limited in many cases from wider use due to high catalyst cost. For example, in the case of biorefining, for the process to be economically viable on a large scale, the turnover number (TON) must be greater than 50,000.[13] Thus, being able to accomplish such transformations with earth-abundant metals would be impactful.

Metals are not only a potential issue from a cost perspective. Having residual catalyst or initiator (in the case of ROMP or REMP) can lead to problems downstream. Polymeric products are particularly susceptible to this issue, as deactivated initiator can easily become trapped in the matrix, creating incompatibilities with certain electronics and biological applications. Significant effort has been expended to address these purification concerns, but they often involve several additional reagents and/or steps, moving these products further away from financial viability.[14] An approach to olefin metathesis, therefore, that avoids metals altogether would seemingly

remove some of the central barriers to wider adoption of this technology, provided that costs associated with it were kept low.

In 2015, such a breakthrough was made by Ogawa et al. out of the Boydston Group when they reported on a redox-based, fully organic system for ROMP, later termed metal-free (MF) ROMP.[15] This was significant, not only from a practical perspective, but also from a fundamental one, since this discovery demonstrated an entirely different system for achieving this transformation than had been seen previously.[16] The initial hypothesis was based on an electrochemical system for cross-metathesis between enol ethers and aliphatic olefins established by the Chiba Group in 2006.[17] In this work, a lithium perchlorate/nitromethane solution was leveraged to enable the anodic activation of an enol ether which could then engage the olefinic metathesis partner (Scheme 1.2a). This outcome is distinct from similar, previous systems that carried out a formal [2+2] cross-coupling between olefins and enol ethers (Scheme 1.2b).[18] It was further determined that olefin functionality could be used to select for either the coupling or metathesis product; sufficiently close electron-donating substituents were shown to support intramolecular electron transfer towards the coupling site, promoting formation of the cyclobutane adduct.[19]
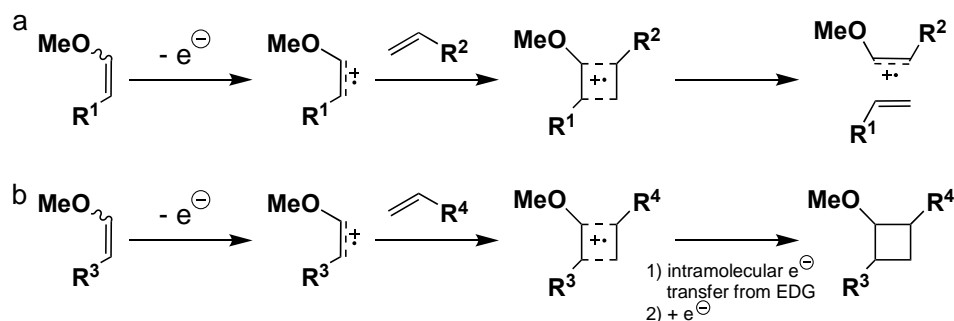

Scheme 1.2. Simplified mechanisms for electrochemical enol ether/olefin a) cross metathesis and b) cross-coupling.

The first attempt at MF-ROMP followed directly from the Chiba work and employed the same electrolyte solution in a polymerization of norbornene with an enol ether as the initiator. Initial results were promising, with detectable amounts of ROMP polymer produced. However,
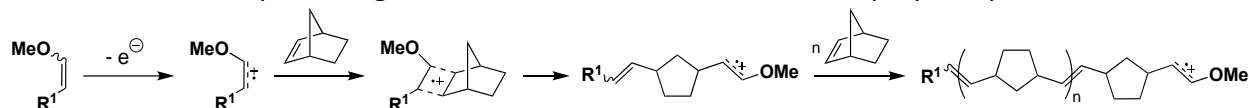
**Scheme 1.3**. Simplified mechanism of MF-ROMP.

monomer conversion was limited to about 3% due to the polymer's insolubility in solution and consequent aggregation on the electrode surface. Engineering solutions such as sonication did not provide much improvement, and so it became apparent that a change in strategy would be necessary. The early 2010s saw much development and expansion of photoredox chemistry, which, as its name suggests, leverages light and light-sensitive molecules to conduct traditionally electrochemical transformations. In contrast to their electrochemical counterparts, these reactions often tout greater solvent compatibilities as well as the benefits associated with homogeneous reactions such as fewer mass transport issues and more versatility in reaction setup (though photochemistry comes with its own idiosyncrasies[20]). Other initially metal-reliant polymerizations have been successfully converted to metal-free systems using photoredox chemistry. Notable examples include organo-catalyzed atom transfer radical polymerization (o-
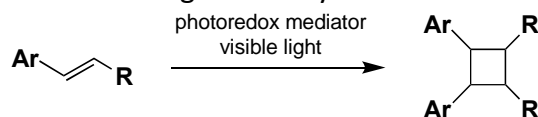
Scheme 1.4. Photoredox-mediated cyclobutane formation.

ATRP), independently established by the Hawker[21] and Miyake[22] groups, and photo-induced electron-transfer reversible addition–fragmentation chain transfer (PET-RAFT) polymerization pioneered by the Boyer group.[23] Our proposed mechanism for MF-ROMP (Scheme 1.3) also alluded to the eventual success of a photoredox-mediated strategy, as the cyclobutane-type intermediate was reminiscent of compounds targeted by the Nicewicz[24] and Yoon[25] groups

(Scheme 1.4) using photoredox mediators like 2,4,6-tris(4-methoxyphenyl)pyrylium tetrafluoroborate and ruthenium tris(bipyrimidine). It was from this work that the first photoredox catalysts for MF-ROMP were selected. For additional details on the selection and behavior of photoredox catalysts in MF-ROMP, please see Chapter 5.
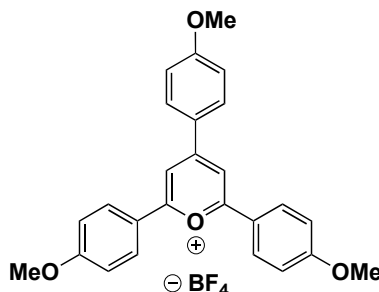
Figure 1.1. Pyrylium photoredox catalyst used in MF-ROMP.

The standard photoredox catalyst (**PC1**) for MF-ROMP was chosen to be 2,4,6-tris(4-methoxyphenyl)pyrylium tetrafluoroborate (Figure 1.1) due to its ease of synthesis and relatively fast conversion of monomer to polymer compared to other pyryliums and thiopyryliums.[15, 26] Blue LEDs were able to be used as the light source for the polymerization, as the λ_{max} of the **PC1** absorbance profile is at 420 nm. The photocontrol of this reaction also enabled demonstration of temporal control with "light on/light off" experiments that showed no significant change in monomer conversion in the dark but continued monomer consumption when irradiation was resumed. A lack of bimodality in the molecular weight distribution of polymer produced in these experiments further demonstrated the ability for the polymer chains to be periodically reduced and oxidized without any significant termination pathways.[15]

While the polymerization was conducted under air-free conditions in the initial report, it was eventually determined that ambient conditions actually resulted in higher monomer conversions over the same time period (80% ± 1% vs 87% ± 2%).[27-28] It was propsed that oxygen may play a role in turning over the photoredox catalyst, though this behavior seems to be more

prevalent in transition metal PCs[27, 29] than for pyranyl radicals.[29] To further complicate matters, MF-ROMP under an atmosphere of oxygen resulted in significantly less monomer conversion (70% ± 4%). The reason behind this observation is not currently well understood, but is being investigated by the group. Please see Chapter 4 for additional related experiments and observations.

In conclusion, MF-ROMP has great potential as an emerging polymerization technology. The initiating system not only circumvents the use of potentially problematic transition metals, but is also greatly reduced in price compared to the standard ROMP initiator; the enol ether and photoredox catalyst average about $600/mol and $7,800/mol, respectively, while the Grubbs third generation initiator is a staggering $430,000/mol. Additionally, while photocontrollable systems for traditional ROMP have been developed using specialized initiators,[7-8] this type of control is already built in to MF-ROMP, affording a number of potential advantages (see Chapter 3). The MF-ROMP initiator system also has a different reactivity profile as a consequence of its different reaction mechanism. Unfortunately this means that monomers with ring strain lower than that of norbornene, which can be readily polymerized using traditional ROMP (e.g., cyclooctene, cyclooctadiene, etc.), are currently unable to be polymerized using MF-ROMP. However, this difference in reactivity also enables capabilities that are not possible in traditional ROMP, such as being able to make linear polymers from monomers with olefinic side rings, such as dicyclopentadiene. These polymers rapidly crosslink under standard ROMP conditions, but can be synthesized with ease using MF-ROMP,[30-31] and even made in flow. Overall, many discoveries regarding this new technology have already been made, but even more have yet to be revealed. This dissertation will explore several of these emerging areas including molecular weight control,

polymer functionalization, and dispersity control. All of these topics, while distinct, contribute to

continually greater applications and understanding of this novel and exciting polymerization.
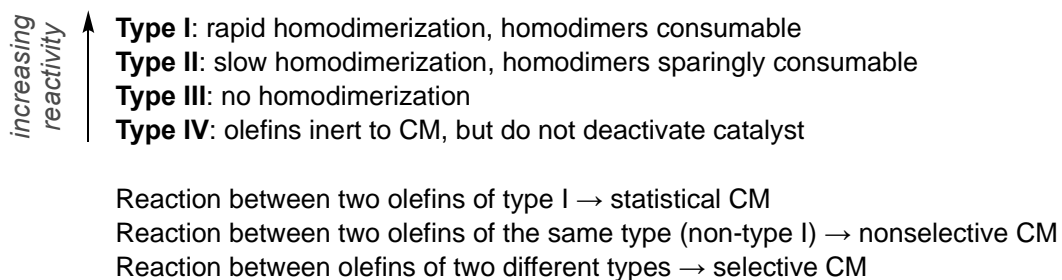
References

1.   Trnka, T. M.; Grubbs, R. H., The Development of L2X2Ru=CHR Olefin Metathesis Catalysts An Organometallic Success Story. *Acc. Chem. Res.* **2001,** *34*, 18-29.

2.   Slugovc, C., Synthesis of Homopolymers and Copolymers. In *Handbook of Metathesis, Volume 3: Polymer Synthesis*, 2nd ed.; Grubbs, R. H.; Khosravi, E., Eds. Wiley-VCH: 2015; Vol. 3, pp 1-23.

3.   Sathe, D.; Zhou, J.; Chen, H.; Su, H.-W.; Xie, W.; Hsu, T.-G.; Schrage, B. R.; Smith, T.; Ziegler, C. J.; Wang, J., Olefin metathesis-based chemically recyclable polymers enabled by fused-ring monomers. *Nature Chemistry* **2021,** *13*, 743-750.

4.   Elling, B. R.; Xia, Y., Living Alternating Ring-Opening Metathesis Polymerization Based on Single Monomer Additions. *J. Am. Chem. Soc.* **2015,** *137*, 9922-9926.

5.   Jeong, H.; John, J. M.; Schrock, R. R.; Hoveyda, A. H., Synthesis of Alternating *trans*-AB Copolymers through Ring-Opening Metathesis Polymerization Initiated by Molybdenum Alkylidenes. *J. Am. Chem. Soc.* **2015,** *137*, 2239-2242.

6.   Neary, W. J.; Kennemur, J. G., Variable Temperature ROMP: Leveraging Low Ring Strain Thermodynamics To Achieve Well-Defined Polypentenamers. *Macromolecules* **2017,** *50*, 4935-4941.

7.   Teator, A. J.; Shao, H.; Lu, G.; Liu, P.; Bielawski, C. W., A Photoswitchable Olefin Metathesis Catalyst. *Organometallics* **2017,** *36*, 490-497.

8.   Theunissen, C.; Ashley, M. A.; Rovis, T., Visible-Light-Controlled Ruthenium-Catalyzed Olefin Metathesis. *J. Am. Chem. Soc.* **2019,** *141*, 6791-6796.

9.   Belov, D. S.; Fenoll, D. A.; Chakraborty, I.; Solans-Monfort, X.; Bukhryakov, K. V., Synthesis of Vanadium Oxo Alkylidene Complex and Its Reactivity in Ring-Closing Olefin Metathesis Reactions. *Organometallics* **2021,** *40*, 2939-2944.

10.   Belov, D. S.; Mathivathanan, L.; Beazley, M. J.; Martin, W. B.; Bukhryakov, K. V., Stereospecific Ring-Opening Methathesis Polymerization of Norbornene Catalyzed by Iron Complexes. *Angew. Chem. Int. Ed.* **2021,** *60*, 2934-2938.

11.   Grau, B. W.; Neuhauser, A.; Aghazada, S.; Meyer, K.; Tsogoeva, S. B., Iron-Catalyzed Olefin Metathesis: Recent Theoretical and Experimental Advances. *Chem. - Eur. J.* **2022,** *28*, e202201414.

12.   Takebayashi, S.; Iron, M. A.; Feller, M.; Rivada-Wheelaghan, O.; Leitus, G.; Diskin-Posner, Y.; Shimon, L. J. W.; Avram, L.; Carmieli, R.; Wolf, S. G.; Cohen-Ofri, I.; Sanguramath, R. A.; Shenhar, R.; Eisen, M.; Milstein, D., Iron-catalysed ring-opening metathesis polymerization of olefins and mechanistic studies. *Nat. Catal.* **2022,** *5*, 494-502.

13.   Stoianova, D.; Johns, A.; Pederson, R., Olefin Metathesis: Commercial Applications and Future Opportunities. In *Handbook of Metathesis, Volume 2: Applications in Organic Synthesis*, 2nd ed.; Grubbs, R. H.; O'Leary, D., Eds. Wiley-VCH: 2015; Vol. 2, pp 699-726.

14.   Vougioukalakis, G. C., Removing Ruthenium Residues from Olefin Metathesis Reaction Products. *Chem. - Eur. J.* **2012,** *18*, 8868-8880.

15.   Ogawa, K. A.; Goetz, A. E.; Boydston, A. J., Metal-Free Ring-Opening Metathesis Polymerization. *J. Am. Chem. Soc.* **2015,** *137*, 1400-1403.

16.   Lu, P.; Kensy, V. K.; Tritt, R. L.; Seidenkranz, D. T.; Boydston, A. J., Metal-Free Ring-Opening Metathesis Polymerization: From Concept to Creation. *Acc. Chem. Res.* **2020,** *53*, 2325-2335.

17.   Miura, T.; Kim, S.; Kitano, Y.; Tada, M.; Chiba, K., Electrochemical enol ether/olefin cross-metathesis in a lithium perchlorate/nitromethane electrolyte solution. *Angew. Chem. Int. Ed.* **2006,** *45*, 1461-1463.

18.   Chiba, K.; Miura, T.; Kim, S.; Kitano, Y.; Tada, M., Electrocatalytic Intermolecular Olefin Cross-Coupling by Anodically Induced Formal [2+2] Cycloaddition between Enol Ethers and Alkenes. *J. Am. Chem. Soc.* **2001,** *123*, 11314-11315.

19.   Okada, Y.; Chiba, K., Electron transfer-induced four-membered cyclic intermediate formation: Olefin cross-coupling vs. olefin cross-metathesis. *Electrochim. Acta* **2011,** *56*, 1037-1042.

20.   Buglioni, L.; Raymenants, F.; Slattery, A.; Zondag, S. D. A.; Noël, T., Technological Innovations in Photochemistry for Organic Synthesis: Flow Chemistry, High-Throughput Experimentation, Scale-up, and Photoelectrochemistry. *Chem. Rev.* **2022,** *122*, 2752-2906.

21.   Discekici, E. H.; Anastasaki, A.; Read De Alaniz, J.; Hawker, C. J., Evolution and Future Directions of Metal-Free Atom Transfer Radical Polymerization. *Macromolecules* **2018,** *51*, 7421-7434.

22.   Theriot, J. C.; McCarthy, B. G.; Lim, C.-H.; Miyake, G. M., Organocatalyzed Atom Transfer Radical Polymerization: Perspectives on Catalyst Design and Performance. *Macromol. Rapid Commun.* **2017,** *38*, 1700040.

23.   Phommalysack-Lovan, J.; Chu, Y.; Boyer, C.; Xu, J., PET-RAFT polymerisation: towards green and precision polymer manufacturing. *Chem. Commun.* **2018,** *54*, 6591-6606.

24.   Riener, M.; Nicewicz, D. A., Synthesis of cyclobutane lignans via an organic single electron oxidant-electron relay system. *Chem. Sci.* **2013,** *4*, 2625-2629.

25.   Daub, M. E.; Jung, H.; Lee, B. J.; Won, J.; Baik, M. H.; Yoon, T. P., Enantioselective [2+2] Cycloadditions of Cinnamate Esters: Generalizing Lewis Acid Catalysis of Triplet Energy Transfer. *J. Am. Chem. Soc.* **2019,** *141*, 9543-9547.

26.   Pascual, L. M. M.; Dunford, D. G.; Goetz, A. E.; Ogawa, K. A.; Boydston, A. J., Comparison of Pyrylium and Thiopyrylium Photooxidants in Metal-Free Ring-Opening Metathesis Polymerization. *Synlett* **2016,** *27*, 759-762.

27.   Lin, S.; Ischay, M. A.; Fry, C. G.; Yoon, T. P., Radical Cation Diels—Alder Cycloadditions by Visible Light Photocatalysis. *J. Am. Chem. Soc.* **2011,** *133*, 19350-19353.

28.   Goetz, A. E.; Pascual, L. M. M.; Dunford, D. G.; Ogawa, K. A.; Knorr, D. B.; Boydston, A. J., Expanded Functionality of Polymers Prepared Using Metal-Free Ring-Opening Metathesis Polymerization. *ACS Macro Lett.* **2016,** *5*, 579-582.

29.   Akaba, R.; Sakuragi, H.; Tokumaru, K., Triphenylpyrylium-salt-sensitized Electron Transfer Oxygenation of Adamantylideneadamantane. Product, Flourescence Quenching, and Laser Flash Photolysis Studies. *J. Chem. Soc., Perkin Trans. 2* **1991**, 291-297.

30.   Goetz, A. E.; Boydston, A. J., Metal-Free Preparation of Linear and Cross-Linked Polydicyclopentadiene. *J. Am. Chem. Soc.* **2015,** *137*, 7572-7575.

31.   Yang, X.; Murphy, L.; Haque, F. M.; Grayson, S. M.; Boydston, A. J., A Highly Efficient Metal-Free Protocol for the Synthesis of Linear Polydicyclopentadiene. *Polym. Chem.* **2021,** *12*, 2860-2867.

Chapter 2: Cross-Metathesis: Molecular Weight Control and Implications for Small Molecule Synthesis

Of the many metathesis reactions outlined at the beginning of Chapter 1, the most visually straightforward is cross metathesis (CM) between two terminal alkenes. The simplicity, however, ends there, as one can readily imagine the great variety of products and product ratios possible depending on the reactivity of both the coupling partners and catalysts employed. Indeed, much work has been done to classify olefins based on their reactivity in transition metal-based CM environments. In general, there are four types (Figure 2.1), initially established by Grubbs et al. according to the olefin's tendency to homodimerize and the reactivity of the subsequent homodimer.[1] This chemical space has been well-explored, and while it is not often the first coupling strategy that most synthetic chemists are drawn to (presumably due to the risk of homodimerization), it has found use in situations where other strategies have failed, particularly where higher functional group tolerance is necessary.[2]

increasing reactivity ↑

Type I: rapid homodimerization, homodimers consumable
Type II: slow homodimerization, homodimers sparingly consumable
Type III: no homodimerization
Type IV: olefins inert to CM, but do not deactivate catalyst

Reaction between two olefins of type I → statistical CM
Reaction between two olefins of the same type (non-type I) → nonselective CM
Reaction between olefins of two different types → selective CM

Figure 2.1. Olefin categories and rules for selectivity.

CM has also seen significant use in the context of ROMP where it is used as a method of chain transfer (CT), which relies on the ability of the active polymer chain-end to undergo metathesis with a linear olefin, creating a "dead" chain and a new initiating species. There are two possible uses for CT in ROMP, and they are not mutually exclusive. The first is to lower the molecular weight of the resulting polymer, which can be a more cost-effective route to oligomers

than simply increasing the loading of the transition metal initiator, which is usually expensive (see Chapter 1). The second is to functionalize the chain end, producing either telechelic polymers (those with functional groups at either chain-end) or heterotelechelic polymers (those with different functional groups at each chain-end) depending on the method employed.[3-4]

We were initially interested in determining if chain transfer between acyclic olefins and active chain ends would be operative in MF-ROMP for both fundamental and practical reasons. From a fundamental standpoint, the ability to demonstrate the similarities and differences between our propagating polymer chains and those of traditional ROMP continues to be of interest to us. More practically, however, we determined early in our investigation of MF-ROMP that low molecular weight (≤ 5 kDa) polymers were difficult to target due to the tendency of the enol ether initiator to undergo cationic homopolymerization at high loadings (≤ 50:1 monomer:initiator). Low molecular weight polymers are of interest due to their many uses in industrial settings, where they can be found as modifiers in resins and composites or as non-volatile alternatives to chemically similar small molecules.[5] (Please see Chapter 3 for additional details about these applications.)
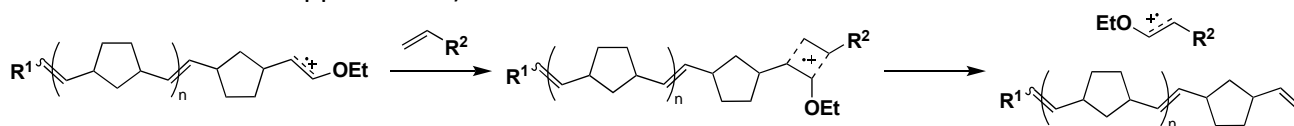
Scheme 2.1. Proposed mechanism of cross metathesis chain transfer in MF-ROMP. See Scheme 1.3 for the mechanism of active chain generation.

Our proposal for the mechanism of chain transfer in MF-ROMP was understandably similar to the mechanism of CT in metal ROMP. We theorized that an acyclic olefin would undergo CM with the active polymer chain end, producing a neutral olefinic chain end and a new, radical cationic enol ether capable of beginning new chains (Scheme 2.1). Though internal acyclic olefins work as chain transfer agents (CTAs) in metal ROMP, we did not observe any significant difference

in final polymer molecular weight in MF-ROMP experiments with added internal olefin. The lower

reactivity towards metathesis of the enol ether radical cation compared to a metal alkylidene is

likely the cause of this difference. However, less sterically hindered terminal olefins (i.e., **1a** and

1b) were found to be effective as CTAs in MF-ROMP, and we observed that altering the

equivalents of CTA afforded us corresponding control over the final polymer molecular weight.

Pulsed addition, necessary in some metal ROMP CT strategies,[6] was happily not necessary here,

and the desired amount of CTA could be added in full at the beginning of the reaction.
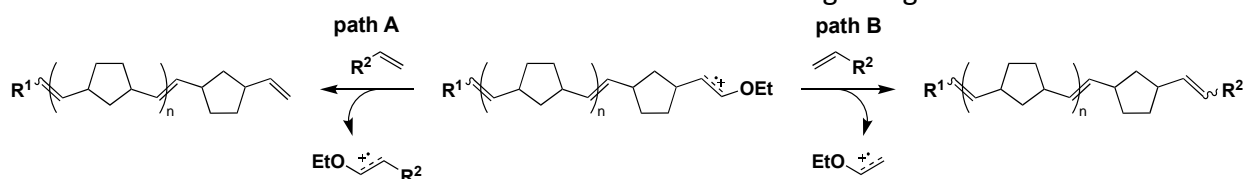
Scheme 2.2. Possible regiochemical outcomes of cross metathesis chain transfer in MF-ROMP.

Additionally, as alluded to in Scheme 2.1, because our CTAs were necessarily asymmetric,

it was possible that the chain transfer events were regioselective. In addition to the products

proposed in Scheme 2.1, another pair was theoretically possible, where the CTA R-group ended

on the polymer chain and the new enol ether initiator had a terminal alkene (Scheme 2.2, path

B). To probe this possibility, ethyl vinyl ether (EVE), the neutral form of the enol ether generated

by theoretical path B, was tested as an initiator in MF-ROMP. In contrast to a polymerization with

ethyl propenyl ether (**2a**, path A, where R^2 = Et), monomer conversion after one hour was 12%

(vs 90%) and the initiator efficiency was 2.8% (vs 66%). This indicated that path A was likely the

dominant one in CM CT for MF-ROMP. This outcome was consistent with the electronic

rationalization that radical cationic enol ether A would preferentaily form over radical cationic

enol ether B, as the more substituted radical cation should be more stable. Additionally, path A

goes through a radical cationic cyclobutane intermediate (Scheme 2.1) that places R^2 in the

sterically favored position opposite the polymer chain; path B would go through a more hindered intermediate where R^2 would be in close proximity to the polymer chain.

Matrix-assisted laser desorption/ionization time-of-flight mass spectrometry (MALDI-TOF MS) confirmed the chain ends as terminal olefins, as predicted by path A. Thus it was proposed that the same terminal alkenes could act as macro CTAs under certain conditions. Indeed, when the amount of added CTA was ≤ 25 equivalents relative to initiator, gel permeation chromatography (GPC) refractive index (RI) traces were bimodal, consistant with chain-chain coupling. This behavior was further evidenced by tracking the polymer distribution as a function of monomer conversion. There, bimodality was not observed until conversion reached 53%.[5] Additionally, CT was determined to occur predominantly at the chain end, as addition of CTA to a polymerization after all monomer had been consumed did not result in a change in polymer molecular weight, but did show a decrease in vinyl ether chain end by ^{1}H NMR spectroscopy.
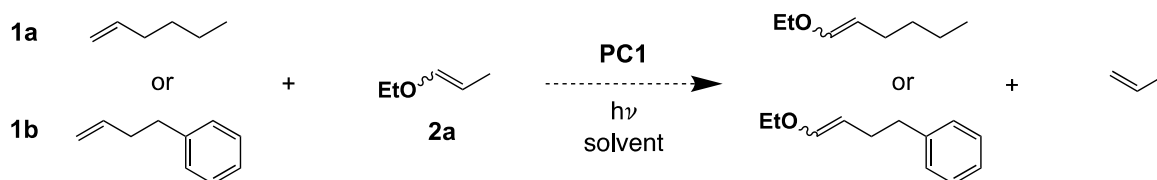
Scheme 2.3. Proposed small molecule photoredox cross metathesis.

This ability to use photoredox chemistry to mediate cross methathesis reactions naturally led us to propose doing such transformations under the same conditions, but with small molecule substrates. Initial experiments were patterned after the Chiba work that inspired MF-ROMP (see Chapter 1) and the successful CTAs (Scheme 2.3).[7] The ratio of enol ether to olefin was widely varied, as was reactant concentration (Table S2.1). However, in each case, oligomerization of **2a** dominated (Figure S2.1 and S2.2). This behavior is consistent with the ability of enol ethers to undergo cationic polymerization. Seeking to limit this behavior, we observed that it is well-

documented that di-β-substituted enol ethers do not undergo cationic polymerization, proposed to be a result of steric hindrance.[8] We proceeded to synthesize such a compound (Figure 2.2) to test in photoredox CM experiments, following similar conditions as before. However, despite the
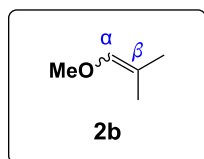

Figure 2.2. Di-β substituted enol ether (methyl-2-methyl-1-propenyl ether) for CM trials.

fact that oligomeriation was successfully prevented, no CM product was able to be detected by ^{1}H NMR spectroscopy; rather, only hydrolysis and acetalization of **2b** were detected (Figures S2.3, S2.4). Significantly, in the Chiba group's electrochemical CM substrate scope, no di-β substituted enol ethers are present, and in their electrochemical cyclobutanation work, product

yields are significantly lower compared to their mono-substituted counterparts.[9] It is therefore possible that the radical cationic forms of di-β substituted enol ethers have low enough reactivity towards CM that no desired products are observed on a reasonable time scale.

In conclusion, there is still much to investigate towards the realization of a photoredox method for small molecule cross metathesis. These initial experiments highlight the nontriviality of this endeavor, but also provide an important jumping-off point for future work. Being able to extend the MF-ROMP strategy into the realm of fine chemical synthesis would be significant, as transformations once only accomplished with expensive transition metals or sensitive electrochemical conditions would be much more accessible. Nonetheless, some changes to the experimentation strategy are needed going forward. Most significantly, mass spectrometry should likely be leveraged to allow for detection of smaller quantities of desired products. ^{1}H NMR spectroscopy, while convenient, is hindered in this case by the strong signal similarities between terminal olefins.

Additionally, the challenges associated with the oligomerization of the enol ether suggest that ring-closing metathesis (RCM) may be a more readily achievable path forward (Scheme 2.4). As concentration is necessaily low for such experiments to favor intramolecular reactions, oligomerization may be largely disfavored. Product detection would also likely be more straightforward than in CM, as a internal olefin will have a significantly different signal in a ^{1}H NMR spectrum, for example, than a terminal olefin.
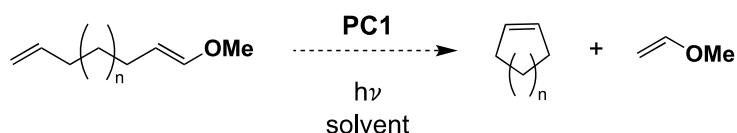
Scheme 2.4. Proposed scheme for metal-free, photoredox ring-closing metathesis.

Though we were not ultimately able to realize this aspirational application of our cross metathesis chain transfer method, we were able to successfully modulate and target polymer molecular weights ranging from 1 to 30 kDa in an inexpensive and operationally simple way. As will be detailed in the next chapter, this method has enabled the development of new materials that will allow the application of MF-ROMP to expand, taking this technology from a pure curiosity to a potentially useful tool.

Experimental Procedures & Supplemental Information

General Considerations: ^{1}H NMR spectra were recorded on a Bruker AVANCE III 400 NMR spectrometer. Chemical shifts are reported in delta (δ) units, expressed in parts per million (ppm) downfield from tetramethylsilane.

General Procedure for Cross Metathesis Trials: To a 7'' NMR tube was added 2,4,6-tris(4-methoxyphenyl)pyrylium tetrafluoroborate (**PC1**, 0.0005 g, 0.001 mmol, 0.01 equiv.) and 1 mL CD_2Cl_2. Solution was vortexed until all **PC1** was dissolved. Olefin (1 – 20 equiv.) and enol ether

(12 μL, 0.1 mmol, 1.0 equiv.) were added. Tube was irradiated with blue LEDs and ^{1}H NMR spectra

were collected for the following time points: dark, 15 min, 30 min, 45 min, 1 hr, 1.5 hr.

Table S2.1. Conditions for initial CM screens. All trials resulted in oligomerization of **2a**. Note that Chiba's electrochemical CM uses 20:1 α-olefin to enol ether.

| [**2a**] (M)	equiv. **2a**	α-olefin	equiv. α-olefin	equiv. **PC1**
0.1	1.0	-	-	0.01
		1b	1.0	
			20	
		1a	1.0	
			20	
0.05		1b	20	0.02
		1a	20	

Procedure for Synthesis of Methyl-2-methyl-1-propenyl ether (**2b**): To a flame-dried flask under

nitrogen was added dry toluene (5 mL) and (methoxymethyl)triphenylphosphonium chloride (6.0

mmol, 1.2 equiv.). Suspension was cooled to –40°C and potassium *tert*-butoxide (6.25 mmol, 1.25

equiv.) was added. Reaction was brought to room temp. over 45 minutes and additional dry

toluene was added (5 mL). To the resulting deep red solution was added acetone (5.0 mmol, 1.0

equiv.), dropwise. Solution stirred at room temperature (21 °C) for 2 hours. Reaction mixture was

then washed with water, dried over sodium sulfate, and fractionally distilled; 42% yield. ^{1}H NMR

(400 MHz, CDCl$_3$) δ 5.64 (m, 1H), 3.43 (s, 3H), 1.50 (d, 3H), 1.44 (d, 3H).
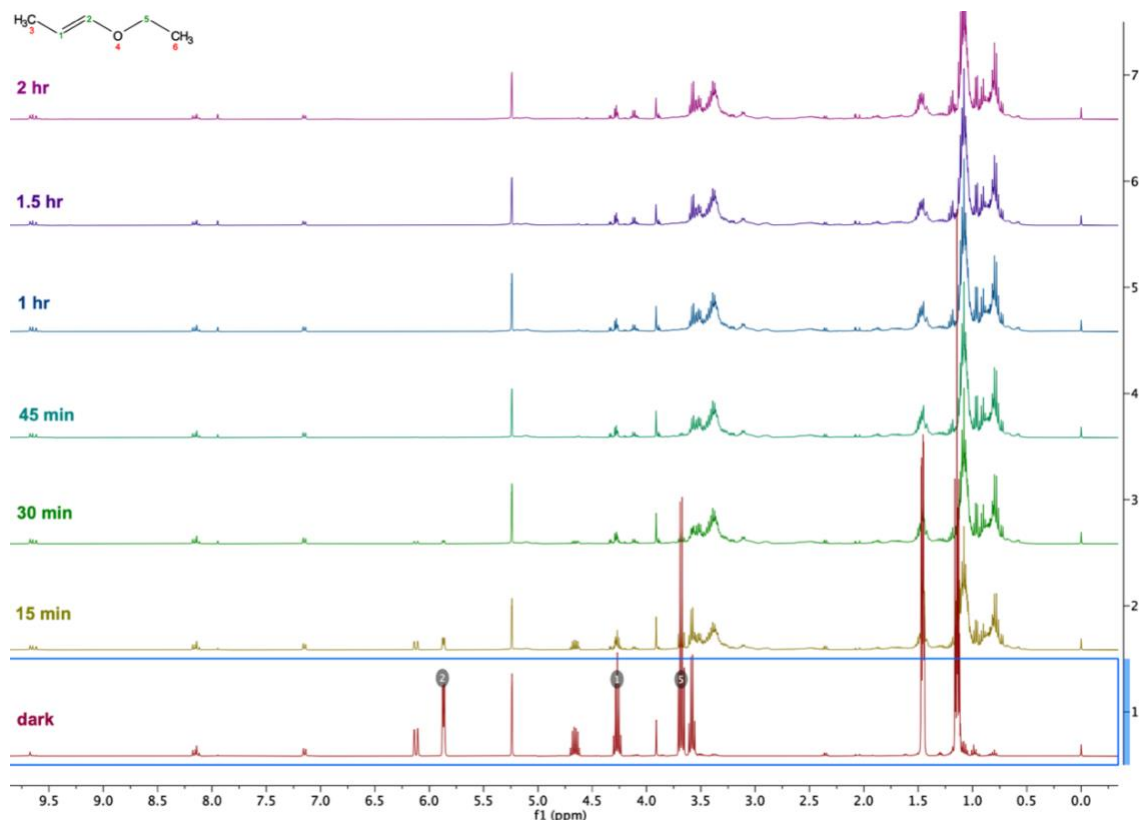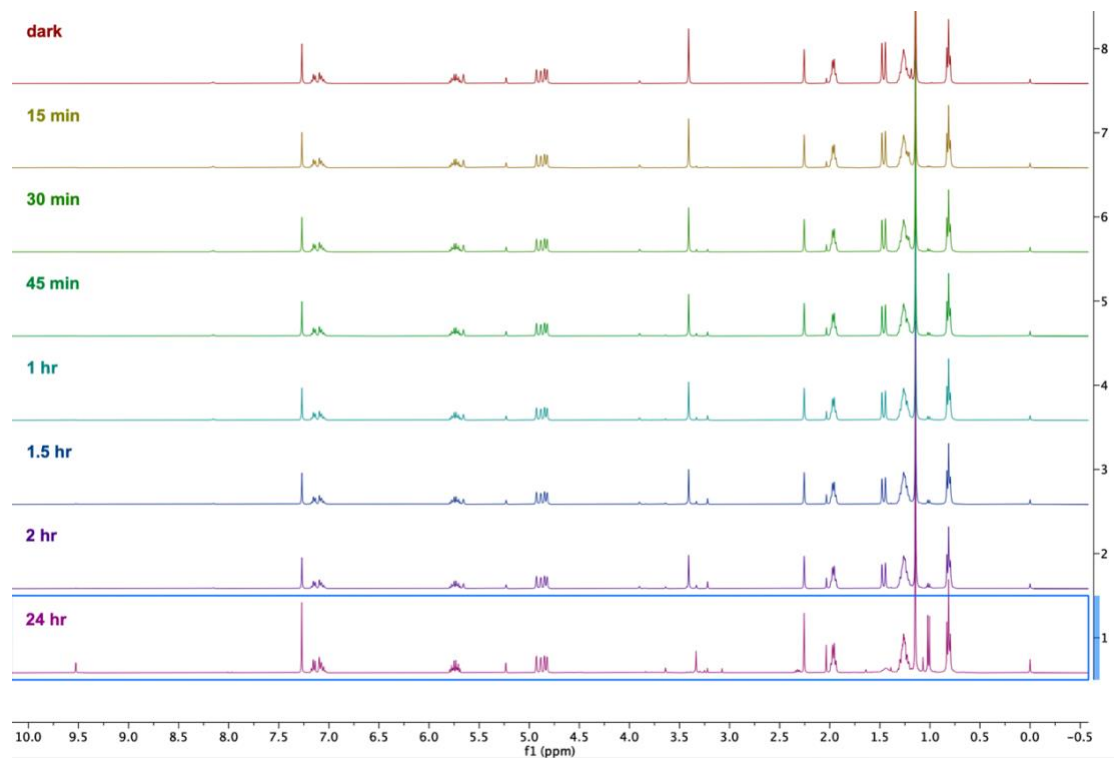
Figure S2.1. Oligomerization of ethyl-1-propenyl ether under photoredox conditions (no terminal olefin present).
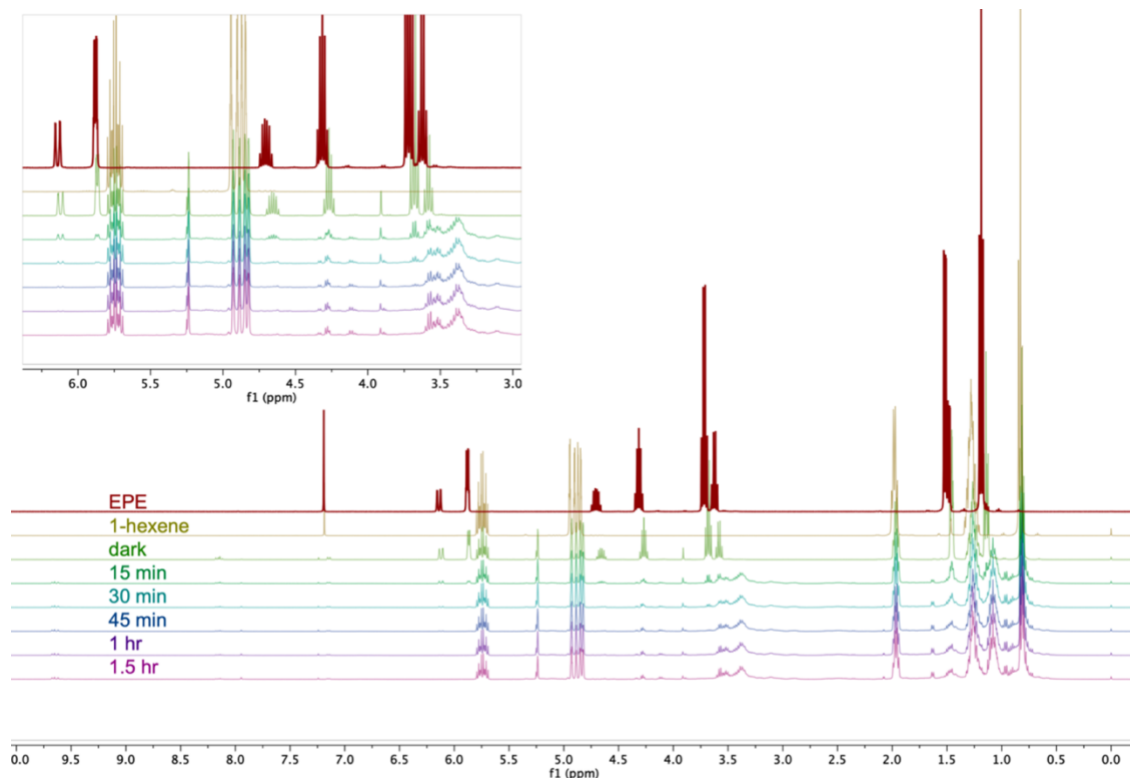
Figure S2.2. Attempted CM of **2a** and **1a**, demonstrating oligomerization of **2a**.
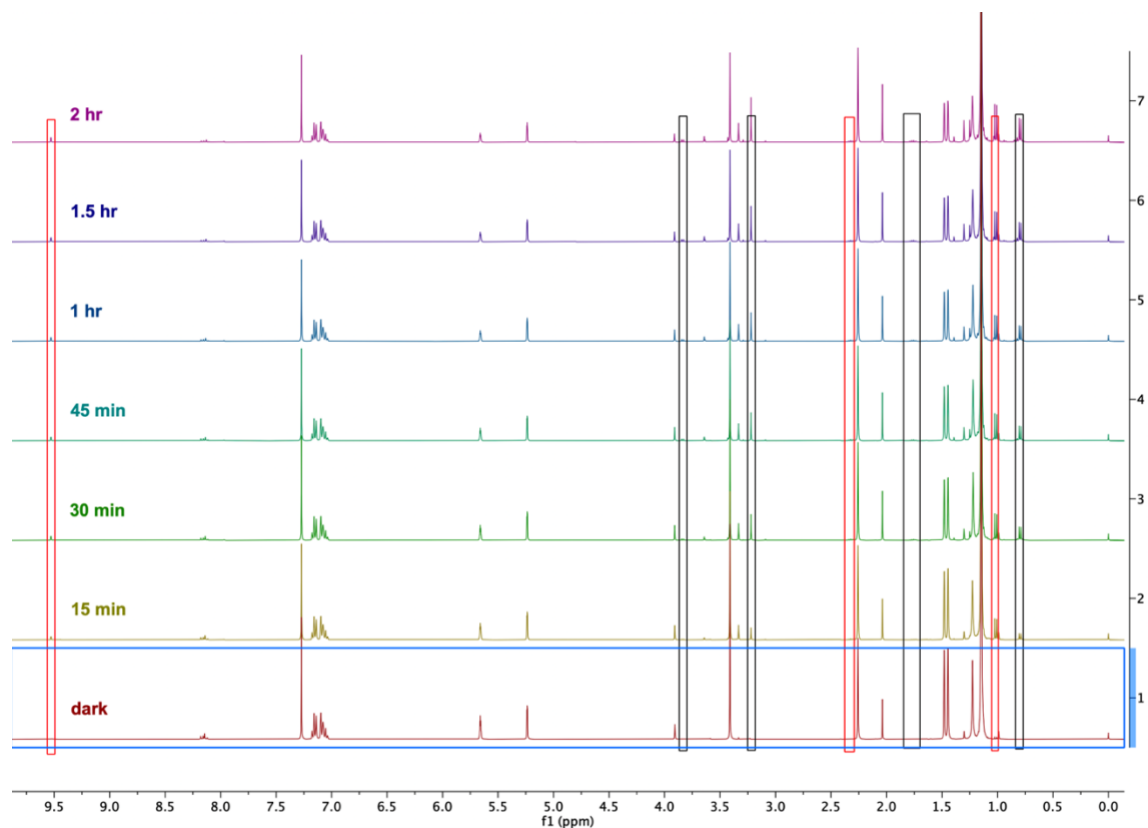
Figure S2.3. Subjection of 2b to photoredox conditions (no α-olefin); red boxes highlight aldehyde signals and black boxes highlight acetal signals.

Figure S2.4. Attempted CM of 1a and 2b; only hydrolysis and acetalization products observed.

References

1.   Chatterjee, A. K.; Choi, T.-L.; Sanders, D. P.; Grubbs, R. H., A General Model for Selectivity in Olefin Cross Metathesis. *J. Am. Chem. Soc.* **2003,** *125* (37), 11360-11370.
2.   Kanada, R. M.; Itoh, D.; Nagai, M.; Niijima, J.; Asai, N.; Mizui, Y.; Abe, S.; Kotake, Y., Total Synthesis of the Potent Antitumor Macrolides Pladienolide B and D. *Angew. Chem. Int. Ed.* **2007,** *46*, 4350-4355.
3.   Michel, X.; Fouquay, S.; Michaud, G.; Simon, F.; Brusson, J.-M.; Roquefort, P.; Aubry, T.; Carpentier, J.-F.; Guillaume, S. M., Tuning the properties of α,ω-bis(trialkoxysilyl) telechelic copolyolefins from ruthenium-catalyzed chain-transfer ring-opening metathesis polymerization (ROMP). *Polym. Chem.* **2017,** *8*, 1177-1187.
4.   Liu, P.; Yasir, M.; Ruggi, A.; Kilbinger, A. F. M., Heterotelechelic Polymers by Ring-Opening Metathesis and Regioselective Chain Transfer. *Angew. Chem. Int. Ed.* **2018,** *57*, 914-917.
5.   Kensy, V. K.; Tritt, R. L.; Haque, F. M.; Murphy, L. M.; Knorr, D. B.; Grayson, S. M.; Boydston, A. J., Molecular Weight Control via Cross Metathesis in Photo-Redox Mediated Ring-Opening Metathesis Polymerization. *Angew. Chem. Int. Ed.* **2020,** *59*, 9074-9079.
6.   Matson, J. B.; Virgil, S. C.; Grubbs, R. H., Pulsed-Addition Ring-Opening Metathesis Polymerization: Catalyst-Economical Syntheses of Homopolymers and Block Copolymers. *J. Am. Chem. Soc.* **2009,** *103*, 283-315.
7.   Okada, Y.; Chiba, K., Electron transfer-induced four-membered cyclic intermediate formation: Olefin cross-coupling vs. olefin cross-metathesis. *Electrochim. Acta* **2011,** *56*, 1037-1042.
8.   Nuyken, O.; Raether, R. B.; Spindler, C. E., Reactivities of substituted acyclic and cyclic enolethers in photoinduced cationic polymerization. *Macromol. Chem. Phys.* **1998,** *199*, 191-196.
9.   Okada, Y.; Yamaguchi, Y.; Chiba, K., Substitution Pattern-Selective Olefin Cross-Couplings. *ChemElectroChem* **2019,** *6*, 4165-4168.

Chapter 3: Silane-Functionalized Materials: Oligomers and Functionalized Nanoparticles for

Impact-Resistant Applications

As noted in Chapter 2, low molecular weight polymers are useful in a number of industrial settings, and after making these materials targetable via the cross-metathesis chain-transfer system, we sought to leverage that value through a collaboration with the Army Research Lab (ARL). Fiber-reinforced composites, a class of impact resistant materials, leverage low molecular weight polymer in the fiber preparation stage. ARL works specifically with composites that use ROMP polymers as the resin base.[1] Before their use in a composite, fibers are coated with a "sizing" mixture. The exact components vary depending on the fiber and bulk resin to be used, but sizing is generally used to protect fibers, make them easier to handle, and, most importantly for this project, improve the properties of the final composite.[2] For glass fibers specifically, the dry sizing package typically consists of a surfactant, a silane, and a film-former. The latter is a low molecular weight polymer that is often more than 80% of the dry sizing mixture by weight. It is especially important that the film former is chemically similar, if not identical, to the chemical composition of the bulk resin, in order to enhance their interactions. This is why our ability to make ROMP oligomers was key to this project. Indeed, as the components of the sizing exist at the interface between the fiber and bulk polymer, it follows that their properties and ability to bridge that interface can have a significant impact on the behavior of the composite as a whole. Previous work by Gorowara et al. has shown that an increase in the percentage of the sizing package unable to be covalently bound to the bulk polymer leads to a reduction in the relative strength retention of the composite.[3]

In fiber-reinforced composites, one main mode of failure is delamination, which is when the resin and the fibers encased within it become separated.[4] One way to mitigate this mode of failure is to enhance the interaction between the resin matrix and the fibers. In a typical sizing package, a large percentage of the components are unable to covalently interact with the bulk resin of the composite. We proposed that if we could produce a film former that incorporates a silane functionality, a large percentage of the sizing package could theoretically be covalently bound to glass fibers in a composite, ideally increasing its relative strength retention.

Table 3.1. Copolymerization of **M1** and **M2**, varying monomer feed ratio.
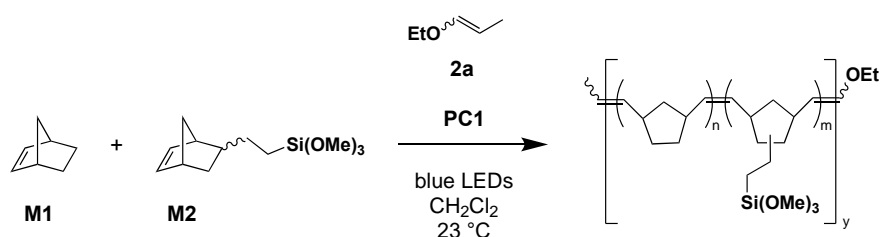

a) Determined by ^{1}H NMR spectroscopy of a reaction aliquot. b) Determined by ^{1}H NMR spectroscopy of the isolated polymer. c) Determined by GPC with in-line multiangle laser-light scattering detection. d) 0.5 M reaction concentration in monomer; all others 1 M. All reaction times = 60 min.

M1:M2	conv.[a]	**M1:M2** (polymer)[b]	M_w[c]	Đ
95:5	76	96:4	19.4	1.4
90:10	71	93:7	18.8	1.3
50:50	23	60:40	14.2	1.5
10:90	0	-	-	-
185:15[d]	47	189:11	13.3	1.4
170:30[d]	43	184:16	13.6	1.3

With this goal in mind, we selected a commercially available, silane-functionalized norbornene (**M2**) to copolymerize with norbornene (**M1**), our model monomer in most MF-ROMP studies. We found that varying the monomer feed ratio enabled us to modulate the amount of silane present in the final polymer (Table 3.1). As the quantity of **M2** relative to **2a** increased, conversion decreased; we hypothesized that a small amount of trimethoxysilane is present in its hydrolyzed form, leading to premature death of 2,4,6-tris(4-methoxyphenyl)pyrylium tetrafluoroborate (**PC1**). This is consistent with empirical observations

as the reaction progresses; the solution is initially bright yellow-green (from **PC1**), but is almost colorless by the end of a **M1/M2** copolymerization. Considering this behavior, it is unsurprising that a feed ratio with predominantly **M2** did not result in a successful polymerization. It is also consistent with the challenges previously documented in attempts to homo- and copolymerize functionalized monomers in MF-ROMP.[5] However, for our purposes, our attainable level of incorporation of **M2** was satisfactory, as a glass fiber sizing package typically contains less than 10% of a silane component, which we were readily able to target.
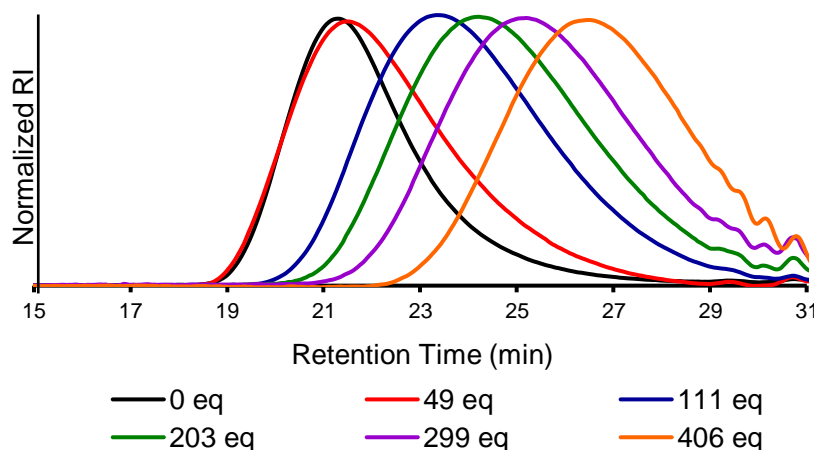

Figure 3.1. Normalized GPC refractive index traces with varied equivalents of CTA **1a** relative to initiator **2a** in a copolymerization of **M1** and **M2**. Polymerization ratio of 170:30:1:0.05 **M1:M2:2a:PC1**.

Following successful incorporation of a silane functionality into our MF-ROMP polymer, we set out to verify the compatibility of copolymerization with our cross-metathesis procedure. Fortunately, we maintained excellent control of molecular weight through CM in the copolymerization of **M1** and **M2** by varying the equivalents of CTA **1a** relative to initiator **2a**, illustrated by stepwise increases in sample retention time in gel permeation chromatography (GPC) experiments (Figure 3.1). We successfully targeted molecular weights as low as 900 Da using this technique (Table S3.1).

To test the utility of these materials, we sought to adhere the silane-functionalized polymers to a model surface. Accordingly, we hydrolyzed the alkoxysilane groups of two **M1/M2** copolymer samples (M_n = 17.3 and 1.34 kDa, Table S3.2) in THF with a small amount of an acetic acid/water solution. We then placed two cleaned and treated silicon wafers in each of the polymer solutions and left them for 24 hours. Upon removal from the solutions, one wafer from each solution was placed directly in an oven under nitrogen at 100 °C, while the other went through a series of sonications before drying (see Supplemental Information for details).

Sessile drop experiments were conducted to determine the relative hydrophobicity of the samples; larger contact angles (θ) correspond to more hydrophobic surfaces. We anticipated that wafers with longer or a greater number of polymer chains on their surface would be more hydrophobic. Indeed, between the sonicated samples, the wafers coated with the higher molecular weight polymer had more hydrophobic surfaces (θ = 76° ± 3°) than those coated with lower molecular weight polymer (θ = 64° ± 5°). The samples that did not go through a sonication step post-polymer adherence were determined to be the most hydrophobic (θ = 91° ± 4° and 88° ± 2°), while all treated wafers were significantly more hydrophobic than the control, where θ = 15° ± 3° (Figure S3.1, Table S3.3).

We also used X-ray photoelectron spectroscopy (XPS) to characterize the wafer surfaces and confirm the sessile drop results. XPS survey scans (Figure 3.1) demonstrated that the sonicated samples were significantly different from the control with respect to surface carbon content (atomic % values in Table S3.4), consistent with polymer chains having been successfully covalently adhered to the silicon surface.
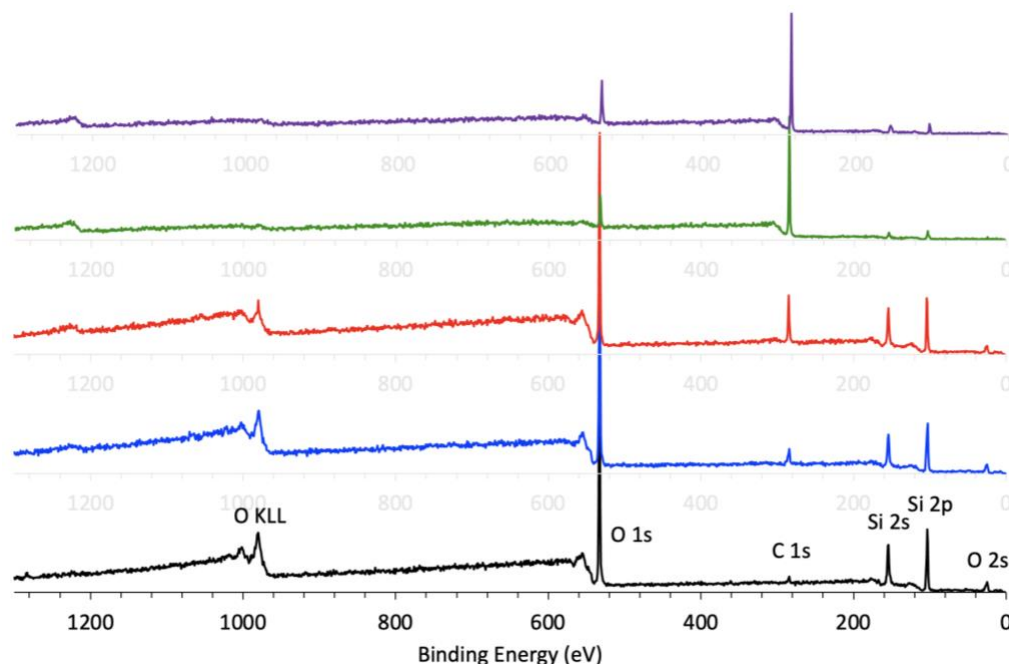
Figure 3.2. XPS survey scans of polymer-coated silicon wafers: control (black), low M_n sonicated (blue), high M_n sonicated (red), low M_n not sonicated (green), and high M_n not sonicated (purple).

Epoxy-functionalized monomer **M3** was also synthesized and tested in a copolymerization with **M1** to illustrate the viability of MF-ROMP as a technique for synthesizing copolymer capable of being adhered to glass surfaces (Table S3.5). We also sought to develop conditions for the copolymerization of **M2** and dicyclopentadiene (**M4**). This was because poly**M4** is a commercially valuable material due to its high chemical, impact, and thermal resistance.[6] It is thus more relevant to the development of fiber-reinforced composites (and of more interest to our ARL collaborators) than poly**M1** materials, which do not share the same material attributes. As mentioned previously, polymerization of monomers other than **M1** via MF-ROMP has been challenging due to the relatively low functional group tolerance of MF-ROMP compared to its metal-based counterpart. Initial investigations into MF-ROMP of **M4** was met with moderate success in that homopolymerization was possible, but challenges were identified. In particular, conversions plateaued around 20% for both the endo and exo forms of the monomer. Because

the forms of **M4** with hydrogenated side rings were able to reach 50% – 90% conversion, it was

hypothesized that the radical cationic active chain end was reacting deleteriously with the alkene

side ring of **M4**.[6]

Table 3.2. Optimization of reaction conditions for copolymerization of **M4** and **M2**. Initial **M4**:**M2**:**2a**:**PC1** of 22:3:1:0.07.


entry	[**M4** + **M2**] (M)	temp. (°C)	time (h)	**M4** conv.[a]
1	1.0	22	1	47%
2	0.5	22	1	31%
3	1.0	3	1	45%
4	1.0	3	2	73%
5	1.0	22	2	54%

a) Determined by ^{1}H NMR spectroscopy of a reaction aliquot. b) Determined by ^{1}H NMR spectroscopy of the isolated polymer.

This problem was eventually resolved by increasing the monomer to initiator ratio and

lowering the reaction temperature. This presumably sufficiently disfavored the undesired side

reaction, but allowed propagation of **M4** to proceed at a reasonable rate.[7] It was with this

information that we proceeded to select ideal conditions for a copolymerization of **M4** and **M2**

(Table 3.2). We again targeted about 10% silane incorporation, but modified monomer to

initiator ratio and reaction temperature to accommodate **M4** as in the aforementioned study.

We found that low temperature and extended reaction times gave the best results (entry 4, Table

3.2), as well as the ideal incorporation of silane functionality (12 mol%). Additionally, under these

conditions, the observed glass transition temperature (135 °C, Figure S3.2) was very similar to

that of a poly**M4** homopolymer of a similar molecular weight (M_n = 10.6 kDa, M_w = 16.3 kDa).[7]

This ability to maintain the material properties of poly**M4** is critical in the context of the desired end-use of the copolymer.
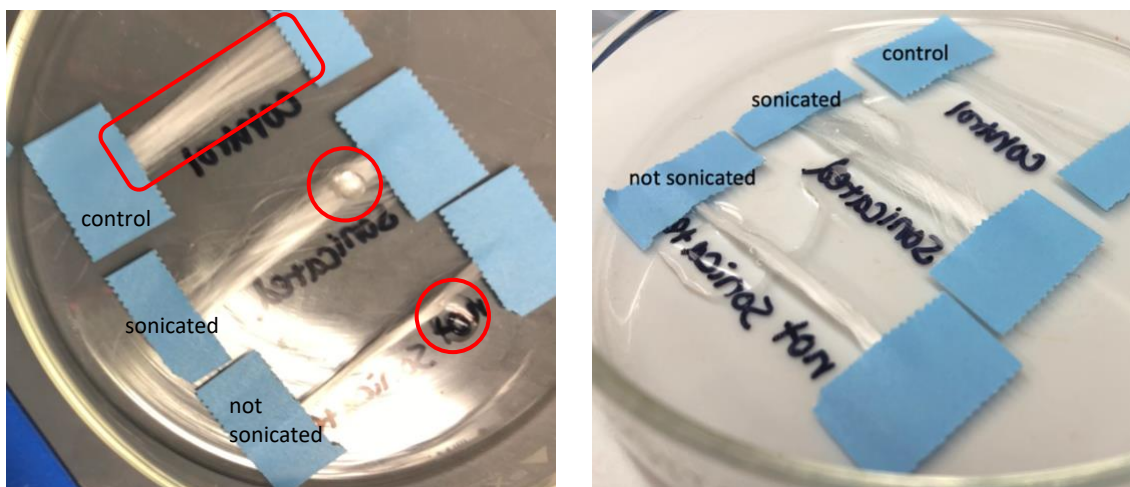

Figure 3.3. Empirical demonstration of differences in hydrophobicity between treated and untreated glass fibers. The control shows full absorption of water amongst the tow fibers, while both the sonicated and non-sonicated samples repel the water. Areas of water exposure are circled on the left image.

We next sought to prove the utility of these materials as fiber coatings called "towpregs" by adhering them to glass fibers. Towpregs serve a purpose similar to the previously mentioned sizing packages in that they are used to make fibers easier to handle and improve their performance in fiber-reinforced composites. The main difference is that fibers are often coated with a towpreg before sale or storage, while sizing packages are usually applied immediately before fiber incorporation. To conduct this material test, we prepared a solution of **M4/M2** copolymer (M_n = 5.13 kDa) in THF and added a 1:9 acetic acid/water solution to hydrolyze the alkoxysilane groups. Two lengths of cleaned ECR glass fiber tows were then added to the solution and left for 24 hours. Upon removal from the solution, one length was immediately placed under vacuum at 40 °C, while the other went through a series of sonications before drying (see Supplemental Information for details). Empirical water drop tests were done to determine relative hydrophobicity of the resulting fibers. Whereas the control fiber tow, which was cleaned

but not exposed to the polymer solution, readily absorbed water along the fibers, water beaded up on the surfaces of the treated tows (Figure 3.3). The apparent hydrophobicity of the polymer-treated and sonicated tow suggests that silane-functionalized polymer has been successfully covalently adhered to the suface of the fibers. While only minor differences were observed between the treated fibers and a control under thermogravimetric analysis (Figure S3.3), this is consistent with the behavior of commercially sized fibers (Figure S3.4).

Having successfully leveraged our silane-functionalized polymers for fiber-reinforced composite applications, we moved to investigating the ability to design a silane-functionalized initiator that could be used for more finely controled material development. Specifically, we were interested in being able to grow ROMP polymer off glass surfaces. So called surface-initiated polymerizations are popular for modifying the surfaces of substrates and nanoparticles for uses as varied as patterned coatings for electronics applications and functionalized particles for reinforcing resin-based materials. In the context of ROMP in particular, polymers have been grown off of silicon wafers and silica particles typically by first adhering a trialkoxysilane monomer to the surface and then attaching the metal alkylidene initiator before polymerizing the desired monomer either in solution or occasionally in the vapor phase.[8-9]
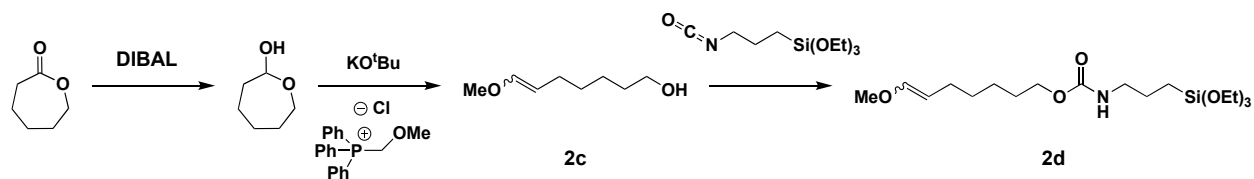
Scheme 3.1. Synthesis of silane-functionalized initiator for surface-initiated MF-ROMP.

Previous work in the group had leveraged a difunctional initiator for the synthesis of a MF-ROMP and ring-opening polymerization (ROP) block copolymer (**2c**).[10] We proposed that this initiator could be readily functionalized to include a trialkoxysilane group using a commercially available trialkoxysilane isocyanate (Scheme 3.1). Indeed, this compound was successfully

synthesized over three steps with moderate yields (steps 1 and 2, 34% overall; step 3, 55%).

Though a variety of functional groups have previously been shown to be incompatible with MF-ROMP, the carbamate tether did not appear to interfere with the activity of initiator **2d**, as the initiator efficiency under standard MF-ROMP conditions was similar to that of **2a** (50% vs 66%; see Supplemental Information for details). This initial success with solution polymerization paved the way for ongoing work that leverages a particular commercially available silica nanoparticle (NP) suspension. Previous studies have used this 30 weight percent dispersion of 12 nm particles in methyl ethyl ketone.[11] This dispersion is distinct from other silica particle suspensions on the market because the NPs are suspended in organic media, rather than water or alcohol. For a graft-from approach, it is critical that the particles are in a mostly aprotic system so as to avoid hydrolysis of the enol ether terminus which will act to initiate the polymerization. With this system, only organic solvents need be leveraged for adherence of the initiators to the particles (Scheme 3.2).
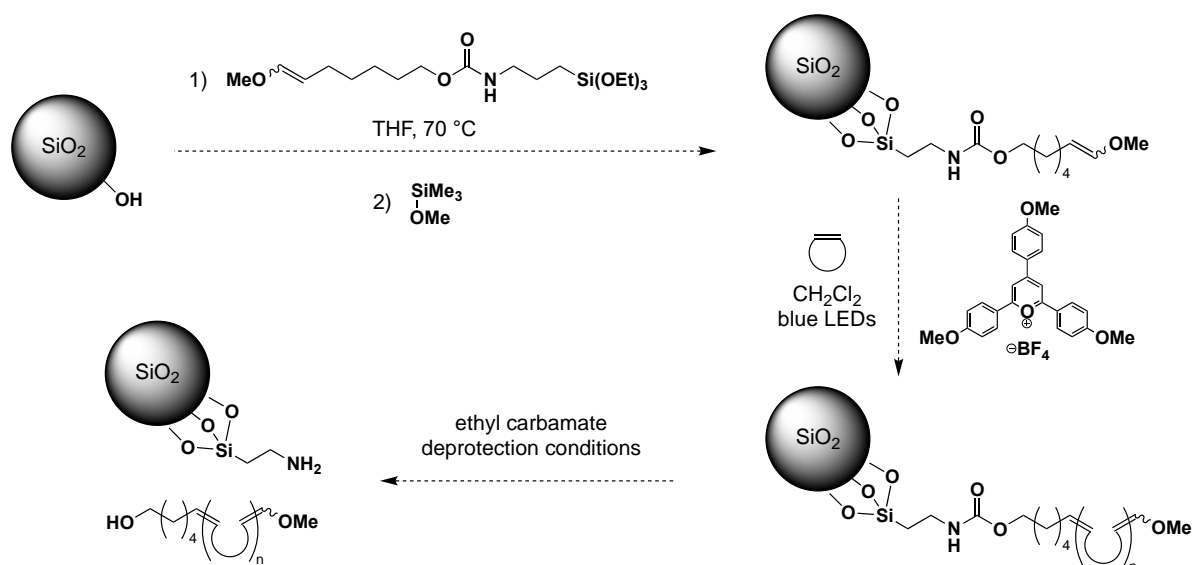
Scheme 3.2. Proposed sequence and conditions for a graft-from approach to producing MF-ROMP-functionalized silica nanoparticles.

A key characterization technique for this study will be dynamic light scattering (DLS), to track the change in particle size over the course of the polymerization. Because we have previously demonstrated that monomer conversion in MF-ROMP can be turned on and off by controlling light exposure, we expect precise control over final graft size to be readily attainable. Additionally, we expect the ability to cleave polymer from the silica core to determine final molecular weight to be more operationally simple than in many current systems (Scheme 3.2). This process is typically conducted in silica-based systems with solutions of hydrofluoric acid.[11] However, the hazards associated with this procedure can be potentially avoided as a function of the carbamate linker which is susceptible to cleavage under certain conditions such as with hydride reductants like Synhydrid, which has been previously used in the deprotection of ethyl carbamates.[12]

The additional capability that can distinguish this work from previous ROMP polymer-functionalized NP syntheses is a function of MF-ROMP itself, which has lower activity towards olefins than traditional, metal-based ROMP. One benefit of this difference, which has been referenced previously, is the ability to polymerize monomers with additional olefinic functionality, such as dicyclopentadiene (**M4**), and avoid crosslinking. In the context of NP functionalization, this is particularly important, as the utility of the material is significantly degraded by particle aggregation. We have also shown previously that metathesis of the backbone is largely avoided in MF-ROMP, making chain-transfer, which could result in unfunctionalized chains and challenges controlling final polymer distribution a likely nonissue. Thus, demonstrating the ability to make poly**M4**-grafted silica NPs via this method will be of key importance.

Developing this system will also pave the way for surface-patterned systems, which can leverage the spatio-temporal control inherent to MF-ROMP as it is mediated by a photoredox catalyst. This could lead to direct uses of MF-ROMP products in the electronics industry, where residual metals make traditional ROMP obsolete. It is also possible that graft density and/or chain length will be able to be controlled using gradiated light, as this has been successfully demonstrated using other photoredox-mediated polymerizations.[13]

In conclusion, the ability to make various silane-functionalized ROMP polymers using our photoredox-mediated, metal-free technique has been demonstrated. This highlights the utility of our polymerization, particularly in the context of producing materials for glass fiber-reinforced materials that leverage our ability to make commercially valuable polymer (poly**M4**) in a linear fashion. This avoids many of the production and application challenges associated with these materials when made with transition metal-based methods. Additionally, we have proposed a readily accessible extension of this work that would enable the development of additonal materials, such as MF-ROMP polymer-functionalized NPs and silicon wafers, that could further expand the applications of this technique.

Experimental Procedures & Supplemental Information

General Considerations: ^{1}H NMR spectra were recorded on a Bruker AVANCE III 400 NMR spectrometer. Chemical shifts are reported in delta (δ) units, expressed in parts per million (ppm) downfield from tetramethylsilane. Gel permeation chromatography (GPC) was performed using a GPC setup consisting of an Agilent 1260 Infinity II pump, 3 in-line columns, and Wyatt miniDAWN TREOS light scattering and Optilab T-rEX refractive index detectors with tetrahydrofuran (THF) as the mobile phase. Number-average molecular weights (M_n) and weight-

average molecular weights (M_w) were calculated from light scattering. All reactions were carried out in standard 2-dram (16.75 mm x 60 mm) borosilicate vials with Teflon caps and were stirred using magnetic Teflon stir bars.

General Procedure for **M1/M2** Copolymerization Trials: To a 2 dram scintillation vial with Teflon cap containing a magnetic stir bar was added **PC1** (0.0006 g, 0.00125 mmol, 0.05 equiv.), 95 to 10 equiv. **M1**, 5 to 90 equiv. **M2**, 5.0 mL CH_2Cl_2, and **2a** (2.8 μL, 0.025 mmol, 1 equiv.). The vial was capped and irradiated with blue LEDs (6W) 1 cm from the vial for 60 minutes. Aliquots were taken for analysis by ^{1}H NMR spectroscopy and GPC and the remaining reaction mixture was filtered through a plug of neutral alumina, eluting with CH_2Cl_2. The solution was concentrated under reduced pressure until a volume of approximately 10 mL remained. The solution was then precipitated into 50 mL of cold, stirring MeOH in an ice bath, and the precipitate was collected via filtration and washed with cold MeOH.

General Procedure for Copolymerization Chain Transfer Trials: To a 5 mL volumetric flask was added **PC1** (0.0003 g, 0.000625 mmol, 0.05 equiv.), **M1** (0.2000 g, 2.125 mmol, 170 equiv.), **M2** (0.0909 g, 0.375 mmol, 30 equiv.), and 0 to 400 equiv. of **1a** measured gravimetrically, and the flask was filled to the line with CH_2Cl_2. This solution was added to a 2 dram scintillation vial with Teflon cap containing a magnetic stir bar and **2a** (1.4 μL, 0.0125 mmol, 1 equiv.) was added. The vial was capped and irradiated with blue LEDs (6W) 1 cm from the vial for 60 minutes. Aliquots were taken for analysis by ^{1}H NMR spectroscopy and GPC and the remaining reaction mixture was filtered through a plug of neutral alumina, eluting with CH_2Cl_2. The solution was concentrated under reduced pressure until a volume of approximately 10 mL remained. The solution was then

precipitated into 50 mL of cold, stirring MeOH in a dry ice/acetone bath, and the precipitate was

collected via filtration and washed with cold MeOH.

Table S3.1. Results of molecular weight modulation with **1a** as CTA with initial **M1:M2:2a:PC1** of 170:30:1:0.1. M_n and M_w values are in kDa.

1a	conv.[a]	M_n[b,c]	M_w[b,c]	$Đ$[b,d]	M_n[c,e]	$M_{n,\,theo.}$	f	CT events per initiator[f,g]	**M1:M2** (polymer)[h]
406	41%	0.926	2.19	2.37	1.98	9.28	469%	3.7	180:20
299	31%	3.01	3.56	1.18	3.06	7.10	232%	1.3	176:24
203	36%	3.44	4.91	1.43	4.47	8.37	187%	0.9	176:24
111	45%	2.74	5.34	1.95	5.29	9.89	187%	0.9	180:20
49	41%	6.88	11.6	1.68	12.1	9.50	78.5%	-0.2	176:24
0	43%	10.1	13.6	1.34	14.5	9.25	63.8%	-	184:16

a)Monomer conversion determined by ^{1}H NMR spectroscopy. b)Determined from crude, unprecipitated reaction aliquots. c)Experimental number-average molecular weight calculated from experimental weight-average molecular weight determined by GPC using multi-angle laser light scattering (MALLS); dn/dc of polynorbornene was used. d)Dispersities determined by GPC analysis. e)Calculated from the peak (maximum peak ± 30 sec.) of the RI trace. f)Initiator efficiency calculated using $M_{n,\,theo.}$ and $M_{n,\,exp.}$ g)No correction was made based on the initiation efficiency calculated in the absence of CTA. h)Determined by ^{1}H NMR spectroscopy of the isolated polymer.

Procedure for Silicon Wafer Preparation: Silicon wafers purchased from UniversityWafer (<100> with a 500 nm thick thermal oxide) were used. Wafers were cut into rectangles (approx. 3 cm x 1 cm), sonicated in a vial of toluene for 10 min, sonicated in a vial of EtOH for 10 min, rinsed with EtOH, and dried with compressed argon; then wafers were treated under UV/ozone for 10 min to remove remaining adventitious carbon. To a THF (15 mL) polymer (0.1 g) solution in a 20 mL scintillation vial with Teflon cap was added 750 μL of a 90:10 acetic acid: deionized water solution. Two wafers were placed in the solution and left for 24 hours. One wafer was removed and placed directly in an oven at 100 °C under nitrogen for 1 hour. The other wafer was sonicated in a vial of toluene for 10 min, sonicated in a vial of EtOH for 10 min, rinsed with EtOH, dried with compressed nitrogen (99.99%), and placed in an oven at 100 °C under nitrogen for 1 hour.

Table S3.2. Molecular weight data for polymer samples adhered to silicon wafers.

M1:**M2**:**2a**:**1a**	conv.[a]	M_n[b]	M_w[c]	Đ[d]	**M1**:**M2** (polymer)[e]
185:15:1:0.05:10	44%	17.3	30.2	1.74	188:12
185:15:1:0.05:300	32%	1.34	1.99	1.48	190:10

a)Monomer conversion determined by ^{1}H NMR spectroscopy. b)Determined from crude, unprecipitated reaction aliquots. c)Experimental number-average molecular weight calculated from experimental weight-average molecular weight determined by GPC using multi-angle laser light scattering (MALLS); *dn/dc* of polynorbornene was used. d)Dispersities determined by GPC analysis. e)Determined by ^{1}H NMR spectroscopy of the isolated polymer.

Table S3.3. Contact angle goniometer measurements. Averages are of five data points except for the control (four).

sample	average	standard deviation
control	15.4°	3
low MW sonicated	63.8°	5
high MW sonicated	75.9°	3
low MW not sonicated	91.0°	4
high MW not sonicated	88.3°	2

**Figure S3.1**. Comparison of contact angle measurements.

Procedure for Sessile Drop Experiments: Static contact angle measurements were conducted using a OneAttension Theta Biolin Scientific Optical Tensiometer in Sessile Drop mode using ultrapure water (resistivity 18.2 MΩ•cm). At least four separate measurements were taken and averaged.

Procedure for X-ray Photoelectron Spectroscopy (XPS) Experiments: XPS was performed on a Physical Electronics VersaProbe II instrument with an Al Kα source. Compositions were obtained

from high resolution scans with a pass energy of 23.5 eV and a step size of 0.05 eV for C 1s, Si 2p,

and O 1s regions. XPS data were processed using CasaXPS software with corrected relative

sensitivity factors from a recent calibration of our XPS.

Table S3.4. Atomic percent values from XPS spectra.

sample	at. % C	at. % O	at. % Si
control	4.4	66.1	29.5
low MW sonicated	9.4	61.4	29.1
high MW sonicated	25.3	49.9	24.8
low MW not sonicated	88.0	8.0	3.9
high MW not sonicated	81.6	12.3	6.1
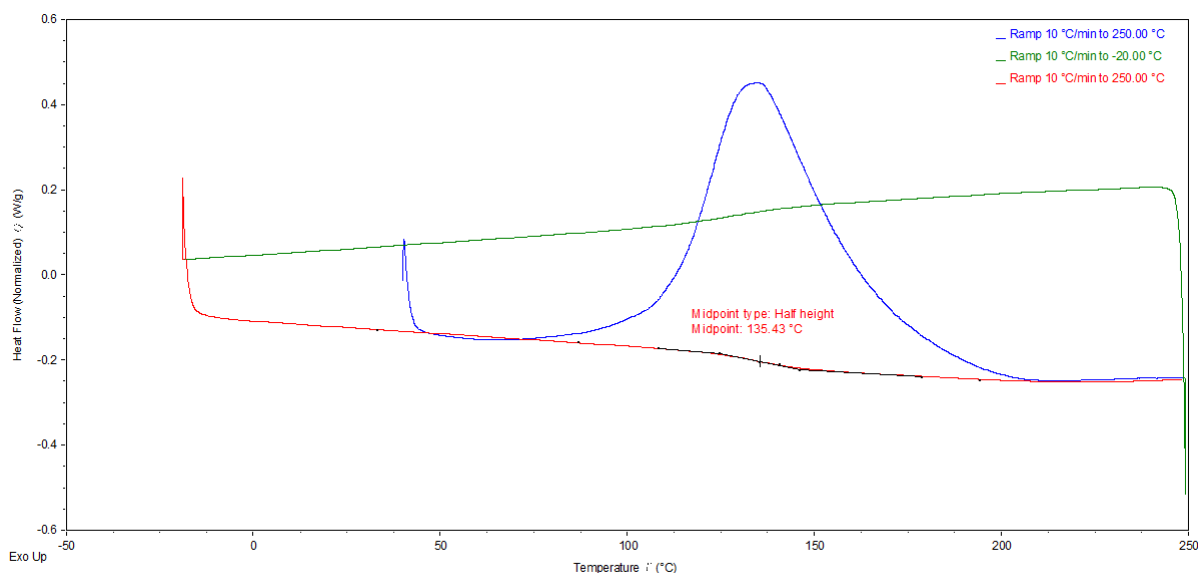
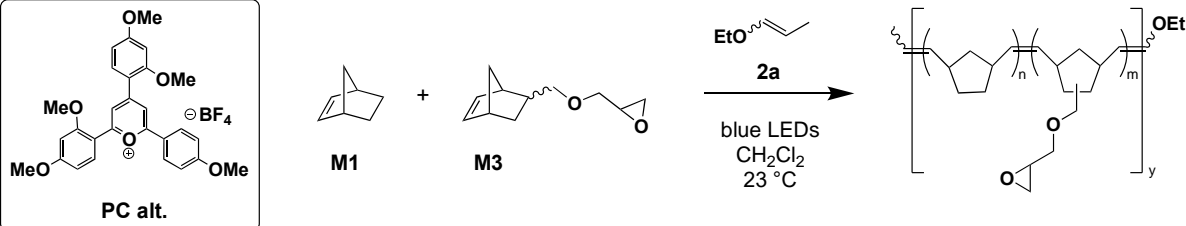**Figure S3.2**. Differential scanning calorimetry data for entry 4 in Table 3.2.
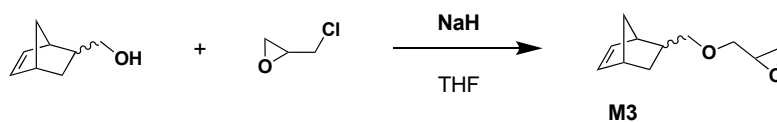
Synthesis of Epoxy-Functionalized Norbornene (**M3**): To a 25 mL flame-dried schlenk flask under

nitrogen was added sodium hydride (60 % in mineral oil; 0.452 g, 11.3 mmol, 1.4 equiv.) and 10

mL dry THF. Suspension was cooled to -78 °C and 5-norbornene-2-methanol (1.0 g, 8.05 mmol,

1.0 equiv.) was added. Solution was allowed to warm to 22 °C over 12 hours. Epichlorohydrin

(0.89 mL, 11.3 mmol, 1.4 equiv.) was added to flask dropwise and allowed to stir for 24 hours.

Reaction was cooled to 0 °C and quenched with saturated ammonium chloride. Reaction mixture was extracted with Et$_2$O, dried over Na$_2$SO$_4$ and concentrated under reduced pressure. Crude mixture was purified using column chromatography (15%→70% EtOAc in Hexanes) giving 53% yield. ^{1}H NMR spectrum consistent with previous literature report.[14]

Table S3.5. Results MF-ROMP of **M1** and **M3**. M_n and M_w values are in kDa.

| **M1:M3:2a:PC1**	[**M1 + M3**]	temp.	time	**M1** conv.[a]	M_n[b]	M_w[c]	$Đ$[d]	mol% **M3** (polymer)[e]
40:10:1:0.07	1.0 M	22 °C	1.25 h	85%	13.6	21.7	1.6	11

a)Monomer conversion determined by ^{1}H NMR spectroscopy; overestimation due to overlap with solvent signal. b)Determined from precipitated sample. c)Experimental number-average molecular weight calculated from experimental weight-average molecular weight determined by GPC using multi-angle laser light scattering (MALLS); dn/dc of polynorbornene was used. d)Dispersity determined by GPC analysis. e)Determined by ^{1}H NMR spectroscopy of the isolated polymer.

Procedure for Glass Fiber Preparation: 1200 tex (17 micron diameter) ECR glass (Advantex TM) provided by Corning was cut into 6" tows and placed in a large glass scintillation vial. The vials were filled with toluene and sonicated for 10 minutes, emptied, filled with ethanol and sonicated for 10 minutes, rinsed with ethanol and dried under an argon stream. A THF/polymer solution (0.47 g polymer in 70 mL THF) was added and 3.5 mL of 1:9 (by volume) acetic acid to water solution was added. After 24 hours, one vial was emptied of polymer solution and placed under vacuum at 40 °C. The other vial was emptied of polymer solution, refilled with toluene, sonicated

for 10 minutes, emptied, filled with ethanol, sonicated for 10 minutes, rinsed with ethanol, and

dried under vacuum at 40 °C.
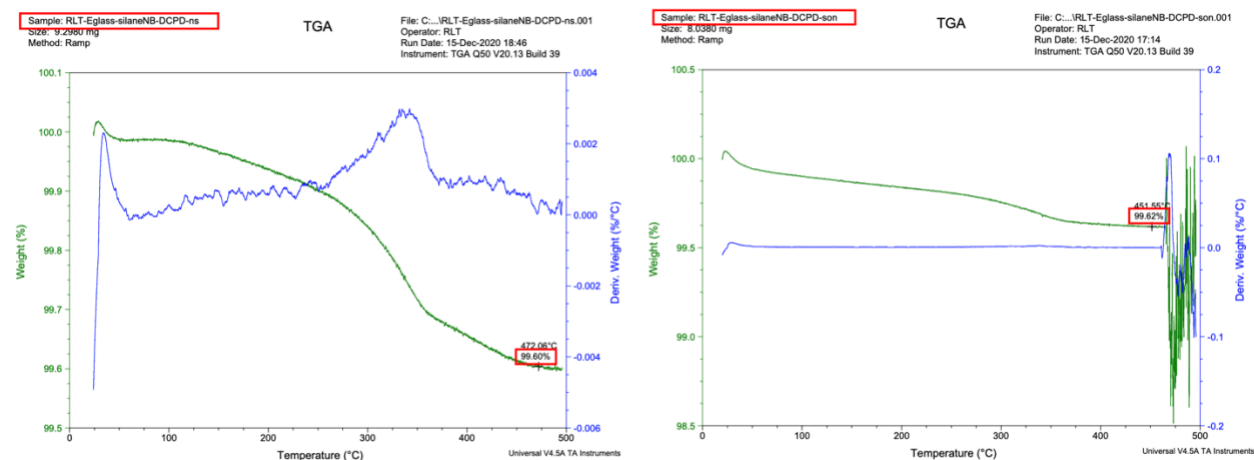
Figure S3.3. Thermogravimetric analysis of sonicated and non-sonicated polymer-coated ECR glass tows.
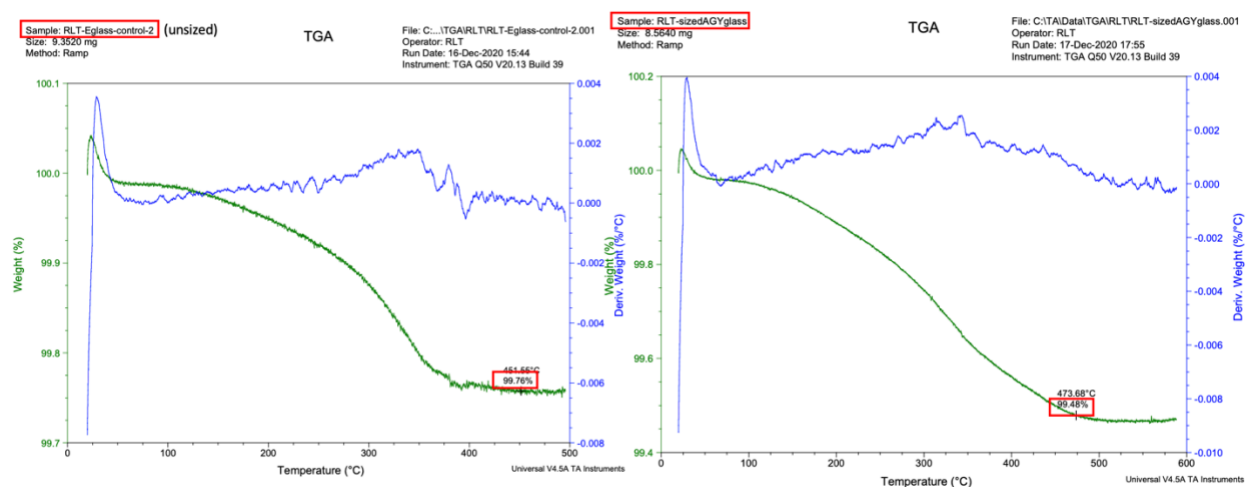
Figure S3.4. Thermogravimetric analysis of control (uncoated) ECR glass tow and commercial sized glass tow.
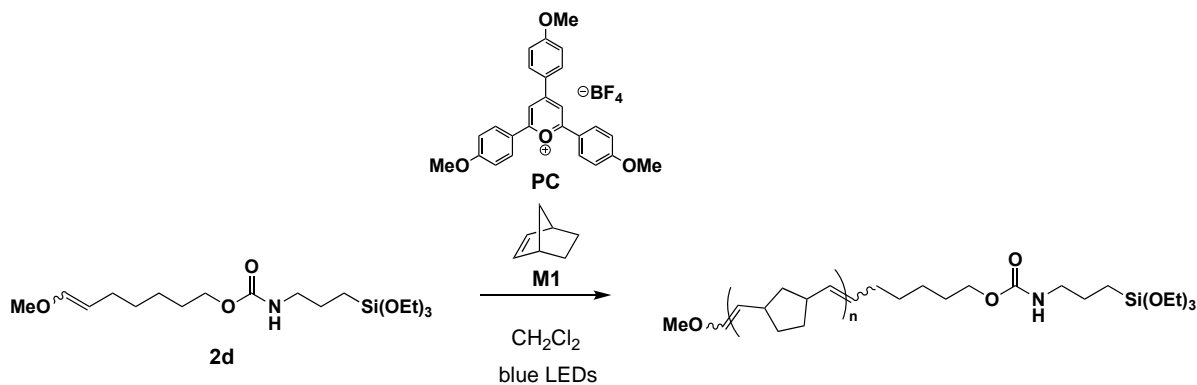
Procedure for MF-ROMP Initiated with Trialkoxysilane-Functionalized Enol Ether (**2d**): To a teflon

cap vial was added **PC1** (0.0012 g, 0.0026 mmol, 0.05 equiv.), **M1** (0.4811 g, 5.11 mmol, 100

equiv.), and 2.0 mL dry CH$_2$Cl$_2$. Solution was stirred in dark until all **PC1** was dissolved. Next, a solution of **2d** (0.051 mmol, 1.0 equiv.) in 0.56 mL dry CH$_2$Cl$_2$ was added. Solution was stirred at 500 rpm and irradiated with blue LED light for 75 minutes. 63% monomer conversion, 50% initiator efficiency, M_n = 12.0 kDa, M_w = 17.7 kDa, Đ = 1.48.

References

1. Boyer, A. J.; Tran, N. T.; Knorr Jr, D. B., Ring-opening metathesis polymerization (ROMP) polymers as structural adhesives and the effects of silane coupling agents on their lap shear properties. *J. Adhes. Sci. Technol.* **2022**.

2. Palmese, G. R.; Andersen, O. A.; Karbhari, V. M., Effect of glass fiber sizing on the cure kinetics of vinyl-ester resins. *Composites Part A* **1999,** *30*, 11-18.

3. Gorowara, R. L.; Kosik, W. E.; McKnight, S. H.; McCullough, R. L., Molecular characterization of glass fiber surface coatings for thermosetting polymer matrix/glass fiber composites. *Composites Part A* **2001,** *32*, 323-329.

4. Patterson, B. A.; Busch, C. E.; Bratcher, M.; Cline, J.; Harris, D. E.; Masser, K. A.; Fleetwood, A. L.; Knorr Jr, D. B., Influence of temperature dependent matrix properties on the high-rate impact performance of thin glass fiber reinforced composites. *Composites Part B* **2020,** *192*, 108009.

5. Goetz, A. E.; Pascual, L. M. M.; Dunford, D. G.; Ogawa, K. A.; Knorr, D. B.; Boydston, A. J., Expanded Functionality of Polymers Prepared Using Metal-Free Ring-Opening Metathesis Polymerization. *ACS Macro Lett.* **2016,** *5*, 579-582.

6. Goetz, A. E.; Boydston, A. J., Metal-Free Preparation of Linear and Cross-Linked Polydicyclopentadiene. *J. Am. Chem. Soc.* **2015,** *137*, 7572-7575.

7. Yang, X.; Murphy, L.; Haque, F. M.; Grayson, S. M.; Boydston, A. J., A Highly Efficient Metal-Free Protocol for the Synthesis of Linear Polydicyclopentadiene. *Polym. Chem.* **2021,** *12*, 2860-2867.

8. Pribyl, J.; Benicewicz, B.; Bell, M.; Wagener, K.; Ning, X.; Schadler, L.; Jimenez, A.; Kumar, S., Polyethylene Grafted Silica Nanoparticles Prepared via Surface-Initiated ROMP. *ACS Macro Lett.* **2019,** *8*, 228-232.

9. Feng, J.; Stoddart, S. S.; Weerakoon, K. A.; Chen, W., An Efficient Approach to Surface-Initiated Ring-Opening Metathesis Polymerization of Cyclooctadiene. *Langmuir* **2007,** *23*, 1004-1006.

10. Lu, P.; Alrashdi, N. M.; Boydston, A. J., Bidirectional metal-free ROMP from difunctional organic initiators. *J. Polym. Sci., Part A: Polym. Chem.* **2017,** *55*, 2977-2982.

11. Zhu, T.; Rahman, M. A.; Benicewicz, B. C., Synthesis of Well-Defined Polyolefin Grafted SiO2 Nanoparticles with Molecular Weight and Graft Density Control. *ACS Macro Lett.* **2020,** *9*, 1255-1260.

12. Lenz, G. R., Synthesis of 7-Oxegenated Aporphine Alkaloids from a 1-Benzylideneisoquinoline. *J. Org. Chem.* **1988,** *53*, 4447-4452.

13.   Li, M.; Fromel, M.; Ranaweera, D.; Rocha, S.; Boyer, C.; Pester, C. W., SI-PET-RAFT: Surface-Initiated Photoinduced Electron Transfer-Reversible Addition–Fragmentation Chain Transfer Polymerization. *ACS Macro Lett.* **2019,** *8*, 374-380.

14.   He, X.; Cheng, C.; Huang, S.; Zhang, F.; Duan, Y.; Zhu, C.; Guo, Y.; Wang, K.; Chen, D., Alkaline anion exchange membranes with imidazolium-terminated flexible side-chain cross-linked topological structure based on ROMP-type norbornene copolymers. *Polymer* **2020,** *195*, 122412.

Chapter 4: Dispersity Modulation: Solvent Effects and Mechanistic Implications

The molecular weight distribution (MWD) of a polymer can have myriad effects on its characteristics such as processing parameters,[1-2] crystallization,[3] and block copolymer self-assembly.[4-5] Different approaches have been taken to control the distribution of polymer chains, including sample blending,[6] metered and modulated reactant addition,[7-10] and mechanism-centered strategies.[11-12] MWD control in ring-opening metathesis polymerization (ROMP) specifically has employed a few different strategies, such as targeted monomer selection[13] and flow reactor design.[14] Metal-free, photoredox mediated (MF) ROMP, which leverages an organic initiator in lieu of the traditional metal alkylidene initiator has recently emerged as an alternative to traditional ROMP, as outlined in Chapter 1. However, as a nascent technology, many aspects of the polymerization are still poorly controlled and understood.[15-16] Recent reports have sought to remedy this, notably the control of molecular weight through cross metathesis chain transfer (see Chapter 2)[17] and stereochemical control via initiator and counterion selection.[18] Control over molar mass dispersity (Đ) in MF-ROMP has remained unrealized.

Understanding this to be an opportunity for development, we looked to previous work on reversible deactivation radical polymerizations (RDRP) for ideas to address it. There, Đ is related to number average degree of polymerization (DP$_n$), monomer conversion (*c*), rate constants of propagation and deactivation (k_p and k_d), inactive polymer concentration, [P], and concentration of deactivator, [D] (Equation 4.1).[19-20] This relationship has been leveraged in the context of many RDRP strategies where greater control over Đ has been sought.

$$Đ = 1 + \frac{1}{DP_n} + \left(\frac{2-c}{c}\right)\left(\frac{k_p[P]}{k_d[D]}\right) \qquad \textbf{(Equation 4.1)}$$

For example, catalyst concentration can be used to modulate dispersity. One such instance was an investigation by the Matyjaszewski group which detailed the behavior of a diblock copolymerization in activators regenerated by electron transfer (ARGET) atom transfer radical polymerization (ATRP). This work varied copper deactivator concentration to target specific dispersities, ranging from 1.32 to 2.0, where higher catalyst concentration corresponded to lower dispersities.[19] This strategy was also demonstrated for iron-catalyzed ATRP by the Anastasaki group, where they were able to maintain monomodal traces even at very low iron concentrations, enabling targeted dispersities from 1.18 up to 1.80.[21] Both of these examples highlight a key characteristic of most well-controlled RDRP: the reliance on an equilibrium between active and inactive chains. This can be gleaned from Equation 4.1, where more inactive chains are often correlated with lower dispersities due to the implied high k_d.

In the context of light-mediated RDRP specifically, work on organocatalyzed atom transfer radical polymerization (O-ATRP) by the Miyake group demonstrated the importance of controlling light intensity to keep dispersities below 1.50. This work proposed that light intensity could be used as an indirect analog for concentration of deactivator, which in O-ATRP is the oxidized photoredox catalyst ion pair. They could also directly control this by changing initial photoredox catalyst concentration.[22]

Significantly, for the majority of examples of dispersity control in RDRP, low dispersities are readily attainable, so the challenge was achieving a controlled increase in Đ. MF-ROMP, in contrast, typically results in polymer dispersities ranging from 1.3 to 1.6 with little apparent control. Thus, we sought to use a similar strategy as was used in previous RDRP studies, but

desired to walk our polymerization closer to the definition of "controlled" by targeting specific $Đ$ values via mechanism-directed reaction engineering.
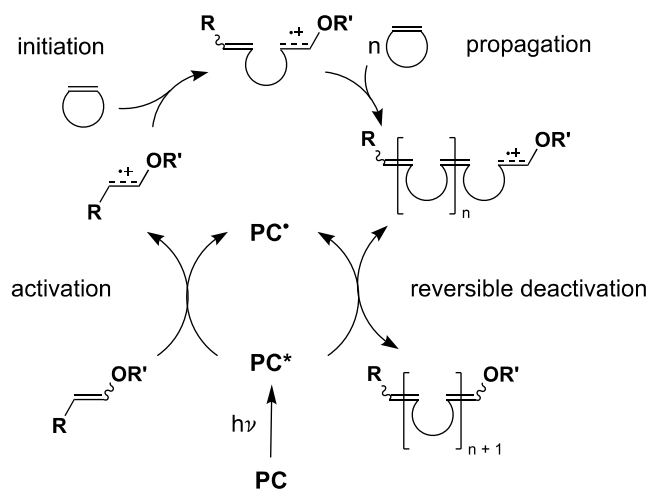

Scheme 4.1. Proposed mechanism of metal-free, photoredox mediated ROMP.

Metal-free, photoredox ROMP is not truly a RDRP, but there is a key similarity which inspired us to adopt strategies associated with controlling the latter in service of the former. This similarity is the reversible deactivation of the active chain-end, demonstrated by "light on/light off" experiments where conversion plateaued in the dark and resumed in the light. During these experiments, the polymer population also remained monomodal, indicating high chain-end fidelity.[16] The central difference then is that the active chain-end in MF-ROMP is not a radical but is instead hypothesized to be a radical cation, due to the behavior of similar small molecule systems.[23-24] This framework is summarized by the generalized mechanism in Scheme 4.1, which represents our current understanding of the system.

Combining this understanding with Equation 4.1, we proceeded to systematically evaluate how different terms may be affected by perturbing reaction conditions. As mentioned previously, a number of aspects of control of MF-ROMP have already been developed, which gave us hints as to how $Đ$ might also be controlled. In particular, our group's use of ion-pairing to

control alkene stereochemistry in the polymer backbone suggested that, among other handles, solvent had a detectable effect on chain-end environment, manifested in *cis* to *trans* ratio.[18] Chain-end environment could also, theoretically, be a handle for controlling k_d (and thus $Đ$) by stabilizing or destabilizing the radical cation.
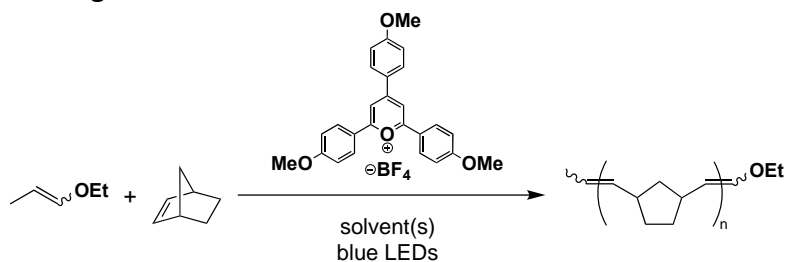

Scheme 4.2. Photoredox mediated ring-opening metathesis polymerization of norbornene.

With this hypothesis in hand, we set about testing the MF-ROMP of a model monomer (norbornene, NB) in a variety of solvent systems with varying degrees of polarity (Scheme 4.2). We supposed that a more polar system should stabilize the radical cation, decreasing k_d and increasing $Đ$. Solvent characteristics can be quantified in a variety of ways (Table S4.1),[25-26] and we tracked both $Đ$ and molecular weight standard deviation (σ) as functions of dielectric (ε), normalized Gutmann donor number (DN^N), and a solvatochromism-based polarity value (E_T^N). In solutions with more than one solvent, we used weighted averages as best estimates.

Across our data series, it was critical that we maintained a consistent degree of polymerization (DP) because $Đ$ is partially a function of DP. As is apparent from Figure 4.1, we were able to maintain DPs that were statistically the same, with one partial outlier (ε = 7.40). This enabled confident data comparison which showed that $Đ$ and σ trended well with ε, while only moderately well with E_T^N and poorly with DN^N (Figure S4.1). As ε values usually correlate with our idea of polarity,[27] the trends we observed with both $Đ$ and σ as functions of ε are consistent with our initial proposal. In general, $Đ$ and σ, which is a function of $Đ$, decreased as ε decreased,

suggesting that changing solution polarity is perturbing the chain-end environment, possibly increasing k_d as ε decreases. While the first three data points have statistically different dispersities (Figure S4.2), interestingly, $Đ$ appeared to plateau as ε decreased past 8.0. We hypothesize that if this change in $Đ$ is an artifact of changing k_d that the plateau denotes that the upper limit of that value is being reached for this system, possibly due to the characteristic rate of interaction between active chain-end and deactivator in solution.
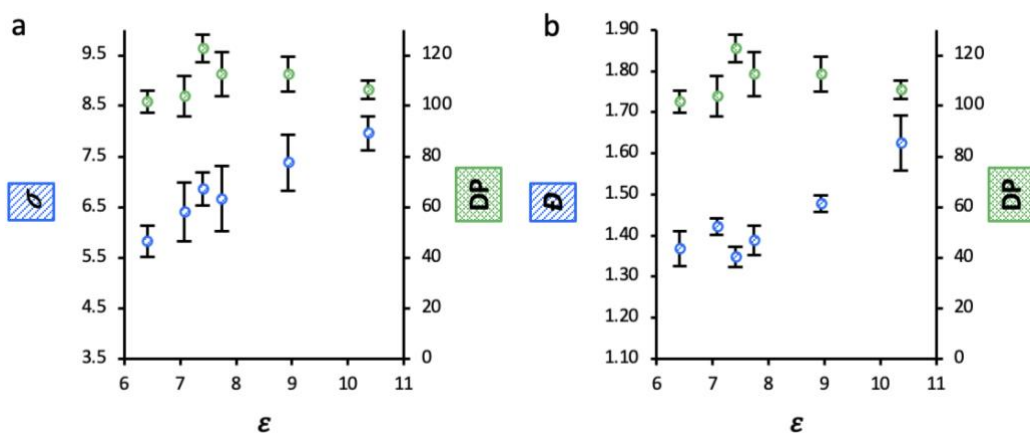
Figure 4.1. Polymer a) standard deviation and b) dispersity tracked as functions of solvent dielectric in MF-ROMP of norbornene with NB:I:**PC1** of 100:1:0.05 and $[NB]_o$ = 2 M, reaction time = 1 hr, temperature = 22 °C. Each data point is an average of six replicates; error bars are one standard deviation.

Importantly, our conversions were also statistically the same or similar across the data series (Table S4.2), though future kinetic studies will also likely be useful in determining how significant of a difference there is in the rates of monomer consumption between solutions. Previous work has demonstrated some difference in this rate as a function of polarity.[17] While it is also possible that the behavior of the pyrylium photoredox catalyst is being affected by the solvent change, we did not observe significant solvatochromism in the solvent systems studied (Figure S4.3), which may suggest that it is not the main contributor to the observed change in polymer growth.
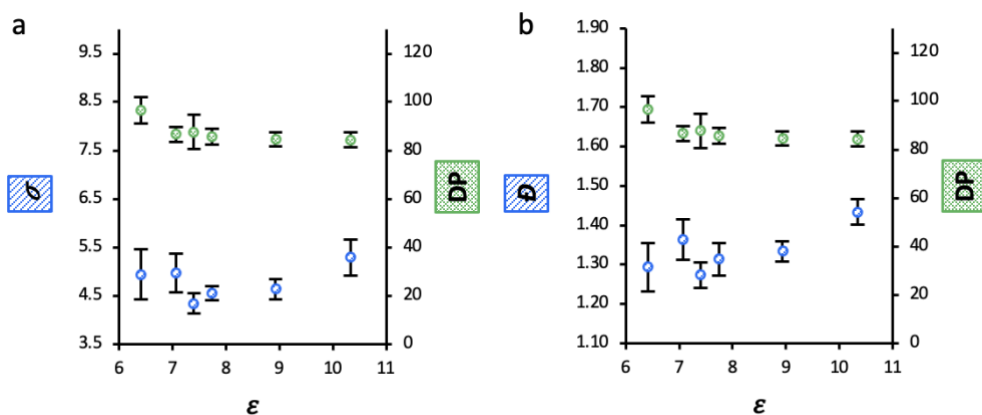
Figure 4.2. Polymer a) standard deviation and b) dispersity tracked as functions of solvent dielectric in MF-ROMP of norbornene with NB:I:**PC1** of 100:1:0.05 and $[NB]_o = 0.5$ M, reaction time = 30 min, temperature = 22 °C. Each data point is an average of four replicates; error bars are one standard deviation.

Due to the apparent limit on increasing k_d using solvent effects, we turned to other terms in Equation 4.1 that we could potentially modulate by changing reaction conditions. One apparently straightforward change to make is polymer concentration, [P], a decrease of which should lead to a decrease in Đ. We tested this proposal by keeping our reagent ratios the same but increasing our solvent volume, changing from an initial monomer concentration of 2 M to 0.5 M. As expected, we observed a significant decrease in dispersity for the lower concentration experiments compared to their higher concentration counterparts (Table S4.3). However, the plateau observed in the previous data series remained and appeared to emerge even earlier, with only the two highest ε value conditions being significantly different from each other (Figure 4.2). Of note is the fact that while the monomer to initiator ratio for these trials is the same as in the previous data set (Figure 4.1), the DPs (and thus also values for σ) are not, due to an apparent increase in initiator efficiency (*f*). It is possible that this is a result of a decrease in the likelihood of deleterious side reactions between initiator molecules and other species due to the lower overall concentration of species in solution. Importantly, though the DPs are significantly lower

due to this increase in f, we can still say that $Đ$ has decreased significantly, as lower DPs ofent

correspond to higher, not lower, dispersities (Table 4.1).

Table 4.1. Effect of reagent concentration on dispersity in MF-ROMP of norbornene.

entry	[NB]$_o$ (M)	solvent vol. (mL)	time (min.)	conv. (%)	DP$_n$	M_n[a]	M_w[a]	$Đ$	σ[b]	f[c] (%)
1	2	2.5	60	80 ± 2	113 ± 8	10.7 ± 0.7	16 ± 2	1.47 ± 0.05	7.4 ± 0.8	73 ± 4
2	2	5	60	67 ± 1	107 ± 8	10.2 ± 0.7	15 ± 1	1.49 ± 0.03	7.1 ± 0.7	63 ± 4
3	0.5	5	30	87 ± 1	86 ± 5	8.2 ± 0.5	11.0 ± 0.7	1.36 ± 0.04	4.8 ± 0.4	93 ± 4

Averages and standard deviations are based upon sets of at least three data points. All reactions were run in dichloromethane with NB:I:**PC1** of 100:1:0.05. Entry one uses the same conditions as entry two in Table S4.2. All entries were run at 22 °C. [a]Values in kDa, determined by gel permeation chromatography (GPC) with multi-angle laser-light scattering (MALLS). [b]$\sigma = M_n\left[(Đ-1)^{1/2}\right]$. [c]Calculated as $(M_{n,\ theo}/M_{n,\ exp})\bullet 100$, taking conversion into account.

Next, we sought to additionally perturb the environment of the active chain-end to

further test our ability to predictably change $Đ$ and ideally lower it below 1.3. 1,1,1,3,3,3-

Hexafluoroisopropanol (HFIP) has been shown to have very unique properties as both a solvent

and as a low-equivalent additive.[28] Much of this uniqueness stems from the fact that it has a high

dielectric constant (ε = 15.7) and low nucleophilicity. This makes HFIP a popular solvent for

generating and studying cations. It has also previously been demonstrated by Shida et al. to have

a significant stabilizing effect on radical cations, enhancing their reactivity in Diels-Alder

reactions.[29] In the aforementioned work, even a small amount of added HFIP (as low as 3.1 equiv.

relative to counterion) resulted in a measurable increase in product yield. They hypothesized that

this was due to HFIP's solvation of the counteranion in solution, as more donating anions had

been observed to inhibit the hole catalysis. Because of this influence on radical cations, we

proposed that adding a relatively small amount of HFIP to the point that dielectric would not be

significantly affected could enhance the reactivity of the active chain-end, resulting in an increase in Đ.

For this experiment, we selected our least polar conditions, hoping that any effect that HFIP has on chain-end stability would be easier to observe, as we would be starting with conditions that typically result in lower relative Đ. Additionally, previous investigations into the active chain-end environment demonstrated that effects are enhanced when ε is low.[18] Indeed, adding only 10 equivalents of HFIP relative to initiator to the solution resulted in a significant increase in Đ (Table 4.2, entry 3). Notably, though HFIP has a high dielectric constant, because such a small amount (2% by volume) was added, the average polarity of the solution was not estimated to change substantially (ε = 6.41 for control and 6.61 for the solution with HFIP). This suggested to us that small amounts of additives may be able to perturb the chain-end environment, displaying effects beyond those related to polarity.

Table 4.2. Effect of additives on dispersity in MF-ROMP of norbornene.

entry	[NB]$_o$ (M)	ε	time (min.)	conv. (%)	DP$_n$	M_n[a]	M_w[a]	Đ	σ[b]	f[c] (%)
1	2	6.41	60	77 ± 1	102 ± 4	9.6 ± 0.4	13.2 ± 0.5	1.37 ± 0.04	5.8 ± 0.3	78 ± 4
2	0.5	6.41	30	89 ± 1	97 ± 6	9.2 ± 0.5	11.8 ± 0.8	1.29 ± 0.06	4.9 ± 0.5	86 ± 5
3*	2	6.61	60	81 ± 3	90 ± 5	8.5 ± 0.5	12.5 ± 0.9	1.46 ± 0.02	5.8 ± 0.5	91 ± 2
4‡	2	7.04	60	72 ± 3	79 ± 2	7.5 ± 0.2	9.2 ± 0.1	1.23 ± 0.03	3.6 ± 0.1	93 ± 6

Averages and standard deviations are based upon sets of at least three data points. All reactions were run in 40 vol% toluene in dichloromethane with NB:I:**PC1** of 100:1:0.05. Entries one and two are from Tables S4.2 and S4.3, respectively. All entries were run at 22 °C. [a]Values in kDa, determined by gel permeation chromatography (GPC) with multi-angle laser-light scattering (MALLS). [b]$\sigma = M_n\left[(Đ-1)^{1/2}\right]$. [c]Calculated as ($M_{n,\ theo}/M_{n,\ exp}$)•100, taking conversion into account. *With 10 equiv. HFIP added (relative to initiator). ‡With 20 equiv. MeCN added (relative to initiator).

In the radical cation Diels-Alder work by Shida et al., the authors also noted that in addition to HFIP promoting the reaction, coordinating solvents like acetonitrile (MeCN) depressed it. We then hypothesized that adding MeCN to MF-ROMP may similarly inhibit reactions with the propagating chain-end, resulting in a lower Đ as a function of lower k_p and/or higher k_d. We again used our lowest polarity conditions to provide direct comparison with the HFIP additive study, and added 20 equivalents of MeCN (2% by volume) relative to initiator. Much to our delight, the dispersity did change significantly compared to the controls, resulting in an average value of 1.23, lower than is typically possible with MF-ROMP, and closer to the ideal of ≤ 1.2 (Table 4.2, entry 4). Interestingly, both experiments with additives resulted in initiator efficiencies that were significantly higher than the controls. It is not immediately clear why this is the case, and more detailed kinetic studies are likely necessary to probe this shift. Indeed, not much is known about why the initiator efficiency in MF-ROMP is typically 60-70%.[17] Because we see good retention of monomodality in "light on/light off" experiments, as mentioned previously, it appears that there is good fidelity once a chain has begun to grow. However, we don't currently have much information about the behavior of initiator molecules early in the polymerization.
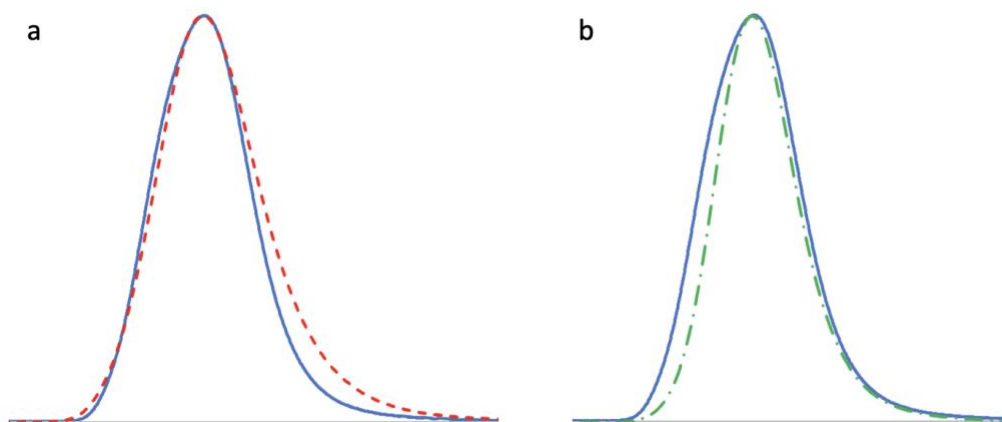
Figure 4.3. Representative GPC normalized RI traces for Table 4.2 a) entry one (solid blue, Đ = 1.34) and entry three (dashed red, Đ = 1.45) and b) entry one (solid blue) and entry four (dashed green, Đ = 1.20). Peaks are overlaid to better illustrate changing Đ. Molecular weight decreases from left to right.

Also of note was the shape of the GPC traces under these different conditions. When HFIP was added to MF-ROMP, the peak appeared to widen on the low molecular weight side compared to the control (Figure 4.3a). When MeCN was added, however, the peak appeared to narrow on the high molecular weight side compared to the same control (Figure 4.3b). It is not immediately clear why this is the case, and detailed kinetic studies are necessary to compare more aspects of these trials. However, based on the current data, it is possible to propose that k_p is increasing with added HFIP and decreasing with added MeCN, which is consistent with these additives' effects on radical cations as noted above; it is also consistent with the effect of these additives on $Đ$ as anticipated by Equation 4.1, as an increase in k_p should result in an increase in $Đ$ and vice versa.

In conclusion, we have explored the effects of solvents and additives in MF-ROMP with the ultimate goal of modulating dispersity using princliples inspired by reversible deactivation radical polymerizations. We revealed that $Đ$ trends well with solvent dielectric, though values appeared to plateau around $\varepsilon = 8.0$. However, we were able to additionally decrease $Đ$ by lowering the reagent concentration, though the previously observed plateau remained. Finally, and perhaps most significantly, we have shown the ability to use low volume amounts of additives to additionally modulate $Đ$. While detailed kinetic studies are necessary in the future to more completely understand these results, we hypothesize that in the case of dielectric effects, the change in $Đ$ was a result of changing k_d. In the case of additive effects, we propose that the change in $Đ$ was a result of changing k_p. Ultimately, we are now able to target dispersites ranging from 1.63 to 1.23, just by changing solvent or using simple additives. This work also serves as an excellent jumping-off point for future studies that seek to elucidate many of the effects on MF-

ROMP that have been observed here, and we look forward to future revelations that may come

of such work.

Experimental Procedures & Supplemental Information

General Considerations: All solvents were dried over 3 Å molecular sieves before use. Norbornene was purchased from Sigma-Aldrich and was fractionally distilled prior to use. 2,4,6-tris(4-methoxyphenyl)pyrylium tetrafluoroborate was prepared according to literature procedure.[30] All other reagents were obtained from commercial sources and used as received unless otherwise noted. ^{1}H NMR spectra were recorded on a Bruker AVANCE III 400 NMR spectrometer. Chemical shifts are reported in delta (δ) units, expressed in parts per million (ppm) downfield from tetramethylsilane. Gel permeation chromatography (GPC) was performed using a GPC setup consisting of an Agilent 1260 Infinity II pump, 3 in-line columns, and Wyatt miniDAWN TREOS light scattering and Optilab T-rEX refractive index detectors with tetrahydrofuran (THF) as the mobile phase. Number-average molecular weights (M_n) and weight-average molecular weights (M_w) were calculated from light scattering. All reactions were carried out in standard 2-dram (16.75 mm x 60 mm) borosilicate vials with Teflon caps and were stirred using magnetic Teflon stir bars. Photochemical reactions were carried out using a modified (no fan) Wisconsin Photoreactor Platform (WPP) equipped with a blue LED star.[31] Light intensity (@455 nm) at 3 cm distance measured with G & R Labs Model 100 Intensity Meter was approx. 24 mW/cm^2 unless otherwise noted.

General Procedure for Polymerizations: To a vial with an oven-dried stir bar was added 4,6-tris(4-methoxyphenyl)pyrylium tetrafluoroborate (**PC1**) and norbornene (NB) gravimetrically. Solvent was added volumetrically, and solution was vortexed until all pyrylium dissolved. Vial was placed in WPP with magnetic stirring (500 rpm) and ethyl-1-propenyl ether (I) was added volumetrically. [2.5 mL solvent volume for 2 M trials and 5 mL solvent volume for 0.5 M trials.] Vial was irradiated

for desired period of time and WPP was covered with lid to omit ambient light. After reaction time had elapsed, light was turned off and a spatula-tip of hydroquinone was added to quench the reaction. A crude aliquot was taken and dissolved in $CDCl_3$ for determination of norbornene conversion by ^1H NMR spectroscopy. An additional crude aliquot was concentrated under reduced pressure and dissolved in HPLC-grade THF for analysis by GPC.

Table S4.1. Polarity, dielectric constant, and normalized donor numbers of solvents used in this study.

| solvent	E_T^N [26]	ε (25 °C) [25]	DN^N [32]
1,2-dichloroethane	0.327	10.36	0
dichloromethane	0.309	8.93	0.026
toluene	0.099	2.38	0.003
chlorobenzene	0.188	5.62	0.09
n-hexane	0.009	1.88	0
1,1,1,3,3,3-hexafluoroisopropanol	1.068	15.70	-
acetonitrile	0.460	37.50*	0.36

*At 20 °C.
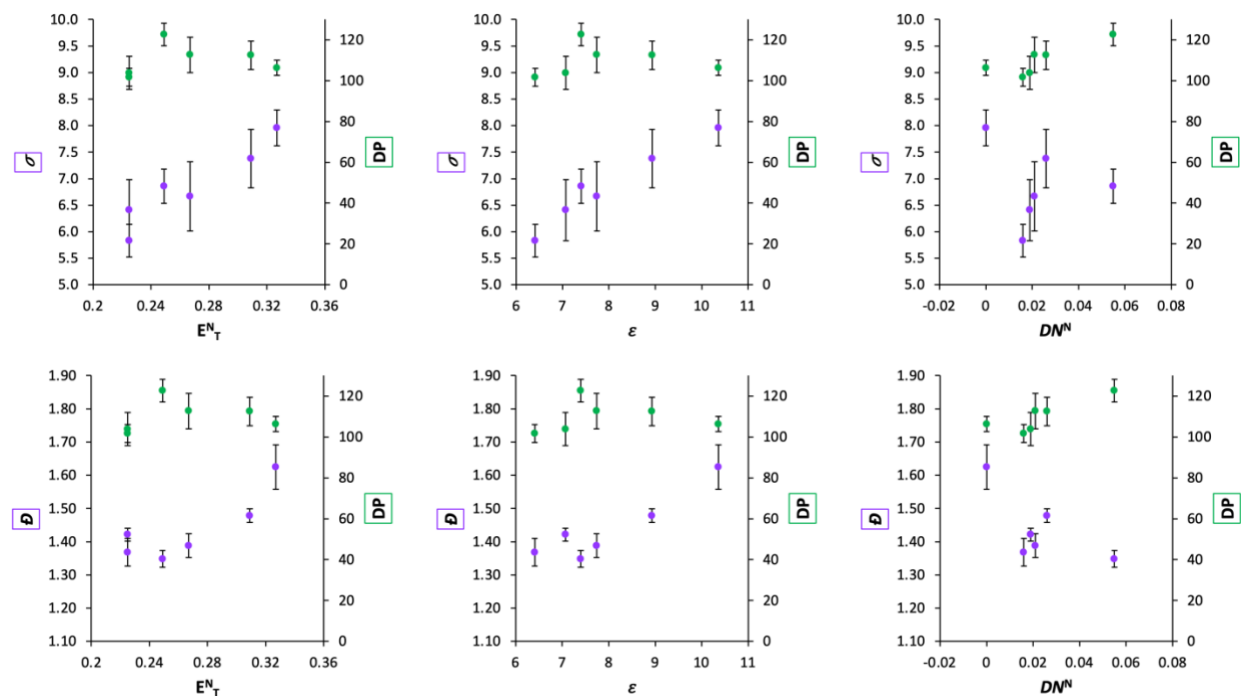
Figure S4.1. Visualization of Table S4.2 data, showing standard deviation and dispersity as functions of different solvent characteristics.
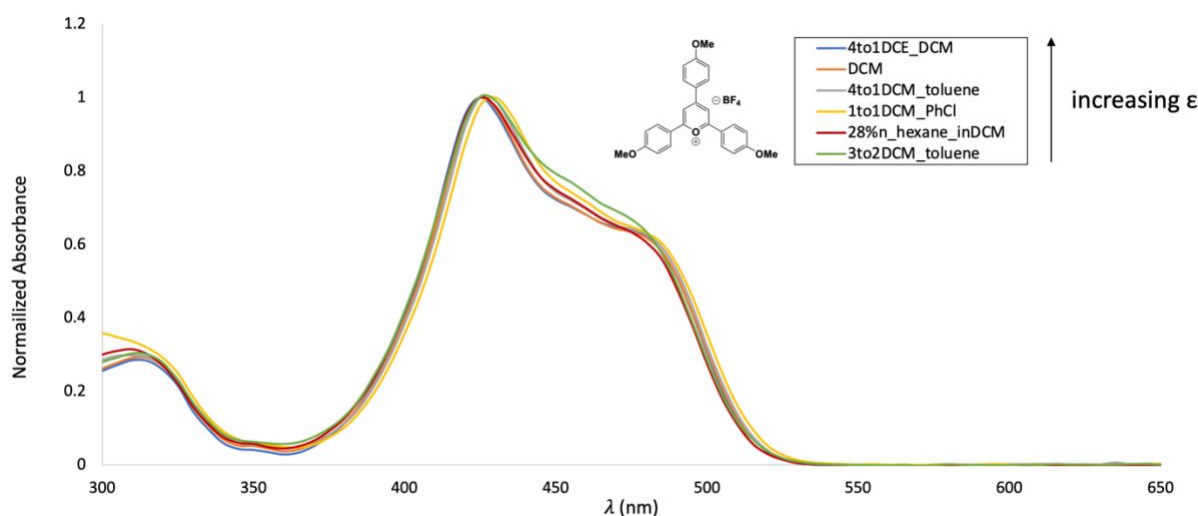
Table S4.2. Detailed data for Figure 4.1; M:I:**PC1** of 100:1:0.05 and $[NB]_o$ = 2 M.

Solvent System	Polarity (E_T^N)	ε	‡DN^N	conv. 1a	DP	M_n^a	M_w^a	Đ	σ^b	f^c	trans:cis†
1,2-dichloroethane	0.327	10.36	0	74% ± 3%	106 ± 4	10.1 ± 0.3	16.4 ± 0.5	1.63 ± 0.07	8.0 ± 0.3	72% ± 5%	79:21
dichloromethane	0.309	8.93	0.026	80% ± 2%	113 ± 7	10.7 ± 0.7	16 ± 1	1.48 ± 0.02	7.4 ± 0.5	74% ± 6%	75:25
4:1 dichloromethane:toluene	0.267	7.74	0.021	76% ± 3%	113 ± 9	10.7 ± 0.8	15 ± 1	1.39 ± 0.04	6.7 ± 0.7	70% ± 8%	78:22
1:1 dichloromethane:chlorobenzene	0.249	7.40	0.055	78% ± 3%	123 ± 6	11.6 ± 0.5	15.7 ± 0.6	1.35 ± 0.02	6.9 ± 0.3	66% ± 4%	77: 23
28% *n*-hexane in dichloromethane	0.225	7.07	0.019	79% ± 1%	104 ± 8	9.9 ± 0.7	14 ± 1	1.42 ± 0.02	6.4 ± 0.6	79% ± 6%	80:20
40% toluene in dichloromethane	0.225	6.41	0.016	77% ± 1%	102 ± 4	9.6 ± 0.4	13.2 ± 0.5	1.37 ± 0.04	5.8 ± 0.3	78% ± 4%	79:21

‡the normalized Gutmann donor number, $DN^N = DN/(38.8\ kcal/mol)$; ᵃin kDa; determined by GPC with MALLS $^b\sigma = M_n[(Đ-1)^{1/2}]$ ᶜcalculated using $M_{n, theo}$ and $M_{n, exp}$; averages and standard deviations are based upon sets of six data points; ε values at 20 °C †from single, representative sample; lack of significant change in trans:cis over series at room temperature consistent with previous report.[18]

a

b
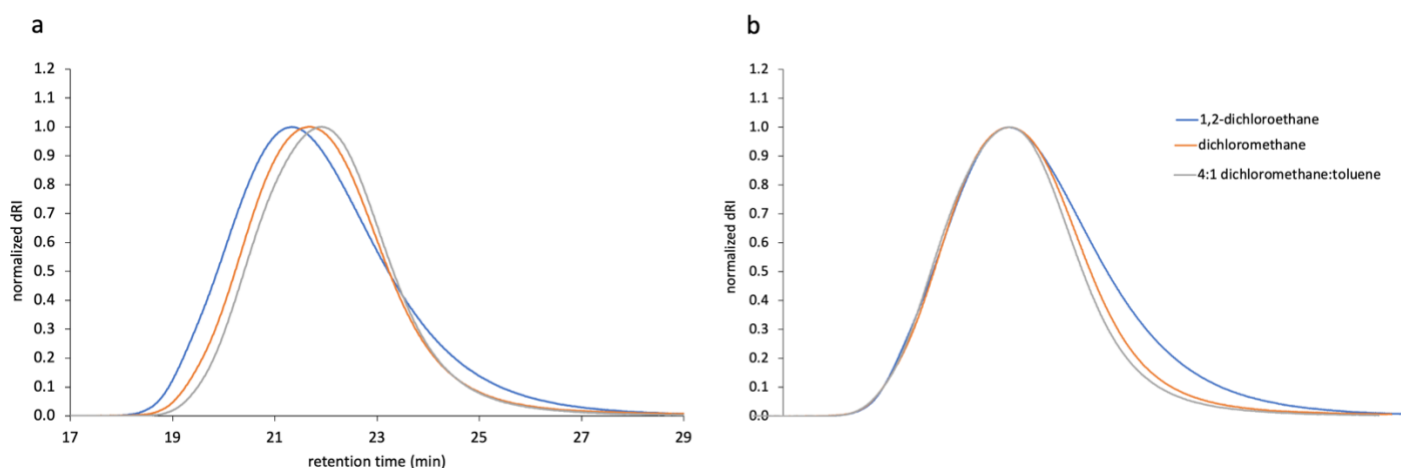
Figure S4.2. Gel permeation chromatography (GPC) normalized refractive index (RI) traces of representative samples for solvent systems with significantly different dispersities, corresponding to the first three entries in Table S4.2 and b) the same traces overlaid to more clearly illustrate the change in Đ.

Figure S4.3 Normalized UV-vis absorbance traces for 2,4,6-tris(4-methoxyphenyl)pyrylium tetrafluoroborate in different solvent systems, demonstrating no significant solvatochromism.

Table S4.3. Detailed data for Figure 4.2; M:I:**PC1** of 100:1:0.05 and $[NB]_o$ = 0.5 M.

Solvent System	Polarity (E_T^N)	ε	‡DN^N	conv. 1a	DP	$M_n{}^a$	$M_w{}^a$	Đ	σ^b	f^c
4:1 1,2-dichloroethane:dichloromethane	0.3234	10.336	0.00515	82% ± 2%	84 ± 3	8.0 ± 0.3	11.5 ± 0.7	1.43 ± 0.03	5.3 ± 0.4	90% ± 5%
dichloromethane	0.309	8.93	0.026	84% ± 1%	85 ± 3	8.0 ± 0.3	10.7 ± 0.4	1.33 ± 0.03	4.6 ± 0.2	93% ± 3%
4:1 dichloromethane:toluene	0.267	7.74	0.021	85%	86 ± 3	8.2 ± 0.3	10.7 ± 0.2	1.31 ± 0.04	4.6 ± 0.1	92% ± 4%
1:1 dichloromethane:chlorobenzene	0.249	7.40	0.055	85% ± 1%	88 ± 7	8.3 ± 0.6	10.6 ± 0.6	1.27 ± 0.03	4.3 ± 0.2	90% ± 7%
28% n-hexane in dichloromethane	0.225	7.07	0.019	85% ± 1%	87 ± 3	8.3 ± 0.3	11.2 ± 0.6	1.36 ± 0.05	5.0 ± 0.4	90% ± 4%
40% toluene in dichloromethane	0.225	6.41	0.016	89% ± 1%	97 ± 6	9.2 ± 0.5	11.8 ± 0.8	1.29 ± 0.06	4.9 ± 0.5	86% ± 5%

‡the normalized Gutmann donor number, $DN^N = DN/(38.8$ kcal/mol); ^{a}in kDa; determined by GPC with MALLS $^b\sigma = M_n[(Đ-1)^{1/2}]$ ^{c}calculated using $M_{n,theo}$ and $M_{n,exp}$; averages and standard deviations are based upon sets of three data points; ε values at 20 °C.

General Procedure for Determination of Polymer Backbone Stereochemistry: Reaction solution was diluted to 2x original volume in dichloromethane and added dropwise to stirring methanol. Suspension was filtered and resulting solids were dried overnight in vacuum oven. A small portion of the dried polymer was then dissolved in CDCl$_3$ for analysis by ^{1}HNMR spectroscopy. See reference 18 for calculations.

References

1. Nadgorny, M.; Gentekos, D. T.; Xiao, Z.; Singleton, S. P.; Fors, B. P.; Connal, L. A., Manipulation of Molecular Weight Distribution Shape as a New Strategy to Control Processing Parameters. *Macromol. Rapid Commun.* **2017,** *38*, 1700352.
2. Sifri, R. J.; Padilla-Vélez, O.; Coates, G. W.; Fors, B. P., Controlling the Shape of Molecular Weight Distributions in Coordination Polymerization and its Impact on Physical Properties. *J. Am. Chem. Soc.* **2020,** *142*, 1443-1448.
3. Tan, R.; Zhou, D.; Liu, B.; Sun, Y.; Liu, X.; Ma, Z.; Kong, D.; He, J.; Zhang, Z.; Dong, X.-H., Precise modulation of molecular weight distribution for structural engineering. *Chem. Sci.* **2019,** *10*, 10698-10705.
4. Widin, J. M.; Schmitt, A. K.; Schmitt, A. L.; Im, K.; Mahanthappa, M. K., Unexpected Consequences of Block Polydispersity on the Self-Assembly of ABA Triblock Copolymers. *J. Am. Chem. Soc.* **2012,** *134*, 3834-3844.
5. Lynd, N. A.; Hillmyer, M. A., Influence of Polydispersity on the Self-Assembly of Diblock Copolymers. *Macromolecules* **2005,** *38*, 8803-8810.
6. Rubens, M.; Junkers, T., A predictive framework for mixing low dispersity polymer samples to design custom molecular weight distributions. *Polym. Chem.* **2019,** *10*, 5721-5725.
7. Parkatzidis, K.; Truong, N. P.; Antonopoulou, M. N.; Whitfield, R.; Konkolewicz, D.; Anastasaki, A., Tailoring polymer dispersity by mixing chain transfer agents in PET-RAFT polymerization. *Polym. Chem.* **2020,** *11*, 4968-4972.

8.   Gentekos, D. T.; Dupuis, L. N.; Fors, B. P., Beyond Dispersity: Deterministic Control of Polymer Molecular Weight Distribution. *J. Am. Chem. Soc.* **2016,** *138*, 1848-1851.

9.   Rosenbloom, S. I.; Sifri, R. J.; Fors, B. P., Achieving molecular weight distribution shape control and broad dispersities using RAFT polymerizations. *Polym. Chem.* **2021,** *12*, 4910-4915.

10.   Corrigan, N.; Almasri, A.; Taillades, W.; Xu, J.; Boyer, C., Controlling Molecular Weight Distributions through Photoinduced Flow Polymerization. *Macromolecules* **2017,** *50*, 8438-8448.

11.   Whitfield, R.; Truong, N. P.; Messmer, D.; Parkatzidis, K.; Rolland, M.; Anastasaki, A., Tailoring polymer dispersity and shape of molecular weight distributions: methods and applications. *Chem. Sci.* **2019,** *10*, 8724-8734.

12.   Morick, J.; Buback, M.; Matyjaszewski, K., Activation–Deactivation Equilibrium of Atom Transfer Radical Polymerization of Styrene up to High Pressure. *Macromol. Chem. Phys.* **2011,** *212*, 2423-2428.

13.   Ahmed, S. R.; Bullock, S. E.; Cresce, A. V.; Kofinas, P., Polydispersity control in ring opening metathesis polymerization of amphiphilic norbornene diblock copolymers. *Polymer* **2003,** *44*, 4943-4948.

14.   Walsh, D. J.; Schinski, D. A.; Schneider, R. A.; Guironnet, D., General route to design polymer molecular weight distributions through flow chemistry. *Nat. Commun.* **2020,** *11*, 3094.

15.   Lu, P.; Kensy, V. K.; Tritt, R. L.; Seidenkranz, D. T.; Boydston, A. J., Metal-Free Ring-Opening Metathesis Polymerization: From Concept to Creation. *Acc. Chem. Res.* **2020,** *53*, 2325-2335.

16.   Ogawa, K. A.; Goetz, A. E.; Boydston, A. J., Metal-Free Ring-Opening Metathesis Polymerization. *J. Am. Chem. Soc.* **2015,** *137*, 1400-1403.

17.   Kensy, V. K.; Tritt, R. L.; Haque, F. M.; Murphy, L. M.; Knorr, D. B.; Grayson, S. M.; Boydston, A. J., Molecular Weight Control via Cross Metathesis in Photo-Redox Mediated Ring-Opening Metathesis Polymerization. *Angew. Chem. Int. Ed.* **2020,** *59*, 9074-9079.

18.   Yang, X.; Gitter, S. R.; Roessler, A. G.; Zimmerman, P. M.; Boydston, A. J., An Ion-Pairing Approach to Stereoselective Metal-Free Ring-Opening Metathesis Polymerization. *Angew. Chem. Int. Ed.* **2021,** *60*, 13952-13958.

19.   Plichta, A.; Zhong, M.; Li, W.; Elsen, A. M.; Matyjaszewski, K., Tuning Dispersity in Diblock Copolymers Using ARGET ATRP. *Macromol. Chem. Phys.* **2012,** *213*, 2659-2668.

20.   Harrisson, S., The downside of dispersity: why the standard deviation is a better measure of dispersion in precision polymerization. *Polym. Chem.* **2018,** *9*, 1366-1370.

21.   Rolland, M.; Truong, N. P.; Whitfield, R.; Anastasaki, A., Tailoring Polymer Dispersity in Photoinduced Iron-Catalyzed ATRP. *ACS Macro Lett.* **2020,** *9*, 459-463.

22.   Ryan, M. D.; Pearson, R. M.; French, T. A.; Miyake, G. M., Impact of Light Intensity on Control in Photoinduced Organocatalyzed Atom Transfer Radical Polymerization. *Macromolecules* **2017,** *50*, 4616-4622.

23.   Riener, M.; Nicewicz, D. A., Synthesis of cyclobutane lignans via an organic single electron oxidant-electron relay system. *Chem. Sci.* **2013,** *4*, 2625-2629.

24.   Okada, Y.; Akaba, R.; Chiba, K., Electrocatalytic Formal [2+2] Cycloaddition Reactions between Anodically Activated Aliphatic Enol Ethers and Unactivated Olefins Possessing an Alkoxyphenyl Group. *Org. Lett.* **2009,** *11*, 1033-1035.

25.   Reichardt, C.; Welton, T., *Solvents and Solvent Effects in Organic Chemistry*. 4th ed.; Wiley-VCH: 2011.

26.   Reichardt, C., Solvatochromic Dyes as Solvent Polarity Indicators. *Chem. Rev.* **1994,** *94*, 2319-2358.

27.   Anslyn, E. V.; Dougherty, D. A., Solutions and Non-Covalent Binding Forces. In *Modern Physical Organic Chemistry*, University Science Books: 2006; pp 145-205.

28.   Colomer, I.; Chamberlain, A. E. R.; Haughey, M. B.; Donohoe, T. J., Hexafluoroisopropanol as a highly versatile solvent. *Nat. Rev. Chem.* **2017,** *1*, 0088.

29.   Shida, N.; Imada, Y.; Nagahara, S.; Okada, Y.; Chiba, K., Interplay of arene radical cations with anions and fluorinated alcohols in hole catalysis. *Commun. Chem.* **2019,** *2*, 24.

30.   Martiny, M.; Steckhan, E.; Esch, T., Cycloaddition Reactions Initiated by Photochemically Excited Pyrylium Salts. *Chem. Ber.* **1993,** *126*, 1671-1682.

31.   Lampkin, P. P.; Thompson, B. J.; Gellman, S. H., Versatile Open-Source Photoreactor Architecture for Photocatalysis Across the Visible Spectrum. *Org. Lett.* **2021,** *23*, 5277-5281.

32.   Cataldo, F., A Revision of the Gutmann Donor Numbers of a Series of Phosphoramides Including TEPA. *Eur. Chem. Bull.* **2015,** *4*, 92-97.

Chapter 5: Initiator and Photocatalyst Scope: Preliminary Investigations and Future Outlook

To understand the chemical space in which metal-free, photoredox-mediated ROMP exists, we must return to our discussion of the small molecule reactions which inspired it from Chapter 1. Specifically, the use of photoredox catalysts has generated much of the inspiriation for the work in this section, and so we will use that to frame our discussion.

Photoredox catalysis has grown over the past few decades to facilitate many unique chemistries, encompassing a broad range of substrates, many of which are unreactive in other synthetic situations.[1] Initial developments focused on transition metal catalysts, predominantly those centered around ruthenium and iridium,[2] but since that time many fully organic photoredox catalysts have emerged. These compounds have been used both in the context of small molecule transformations, such as alkylations, aminations, halogenations, cycloadditions, and cycloreversions,[1] as well as in controlled polymerizations.[3] In the context of MF-ROMP, photoredox catalysts used in cycloadditions are of most interest, becuase the transformation that is proposed to be occurring during the initiation step is a cycloaddition (Scheme 1.3). In such work, radical cations are generated from the one electron oxidation of an alkene; [2+2],[4-6] [4+2],[7-8] and even [6+4][9] cycloadditions have been demonstrated in this context, with [2+2] being most relevant to our work.

Previous studies by the Nicewicz group specifically used 2,4,6-tris(4-methoxyphenyl)pyrylium tetrafluoroborate (**PC1**) to conduct [2+2] cycloadditions.[5] Indeed, as discussed in Chapter 1, this is some of the precedent that inspired us to attempt the redox step of MF-ROMP with a pyrylium photoredox catalyst when barriers were encountered in the electrochemical conditions. In the Nicewicz work, however, it is not enol ethers that are oxidized

to radical cations as in MF-ROMP, but the aromatic molecule anethole (**3**), as well as other aromatic alkenes. This suggested to us that anethole could be an alternate initiator in MF-ROMP. Expanding the initiator class was of interest to us because it would instill more versatility in our polymerization, potentially allowing us to circumvent some of the issues associated with enol ethers (Chapter 2). Unfortunately, when such a reaction was attempted (Table 5.1, entry 2), no polymer was detected by ^{1}H NMR spectroscopy. However, in the small molecule work it was noted that electron relays (ER) such as anthracene or naphthalene were necessary to prevent cycloreversion, and so initiation with anethole was re-attempted with added ER (**4**).

Table 5.1. Controls for and attempts with anethole as an initiator for MF-ROMP.

entry	2a[a]	3[a]	4[a]	time (hr)	conv. (%)[b]	f[c] (%)
1	1.0	-	-	1	81	63
2	-	2.0	-	18	n.d.	-
3	1.0	-	0.5	1	86	59
4	1.0	-	2.0	1	84	59
5	-	2.0	0.5	22	n.d.	-

M1:I of 100:1 for all trials; 0.05 equiv. **PC1** used with **2a** and 0.03 equiv. **PC1** used with **3**. [a]Molar equivalents. [b]Determined by ^{1}H NMR spectroscopy. [c]Calculated as $(M_{n,\ theo}/M_{n,\ exp})\bullet100$, taking conversion into account.

When this attempt also resulted in no detectable monomer conversion by ^{1}H NMR spectroscopy (Table 5.1, entry 5), it was noted upon closer inspection of the small molecule work that the highest yield of cycloaddition product from anethole (54%) was after a reaction time of five days. In our envisioned mechanism, this cycloaddition must be happening each time a monomer is added to the growing polymer chain, and so it was proposed that if any monomer was being consumed, it was too slow to be detected even after over 20 hours of reaction time (in the Nicewicz work, 18% cycloaddition product was observed after one day).

Having been unable to initiate MF-ROMP with anethole using a pyrylium PC, we turned

to work on photoredox-catalyzed cyclobutanations by Tanaka et al., which offered some

suggestion of a path forward in expanding the initiator class in MF-ROMP to potentially include

aromatic alkenes. This work similarly demonstrated a [2+2] cycloaddition with anethole but

leveraged a different photoredox catalyst: a thioxanthylium.[6] While the catalyst used has a

similar excited state reduction potential (E^*_{red}) to **PC1** (1.76 V vs SCE compared to 1.89 V vs SCE

for **PC1**),[10] its λ_{max} occurs at slightly longer wavelengths (515 nm compared to 425 nm for **PC1**).

This allows lower energy green light to be used instead of blue. Additionally, and most

importantly, over 99% conversion to the cyclobutane adduct was recorded using this photoredox

catalyst with a reaction time of only two hours.

Table 5.2. Controls for and attempts with anethole as an initiator for MF-ROMP
with a thioxanthylium photoredox catalyst.

entry	**M1**[a]	**2a**[a]	**3**[a]	styrene	time (hr)	temp. (°C)	conv. (%)
1	100	1.0	-	-	2	23	trace
2	100	-	1.0	-	2	23	n.d.
3	-	-	1.0	10	2.2	23	30*
4	10	-	1.0	-	2.2	23	n.d.
5	10	-	1.0	-	2.2	50	n.d.

M1:I:**PC2** of 100:1:0.02 for all trials. [a]Molar equivalents. [b]Determined by [1]H
NMR spectroscopy. [c]Calculated as ($M_{n, theo}/M_{n, exp}$)•100, taking conversion
into account. *Cyclobutane product.

To explore the possibility of using a thioxanthylium as a photoredox catalyst in MF-ROMP,

we synthesized such a compound that had a similar E^*_{red} to **PC1**. **PC2** is reported to have an E^*_{red}

of 1.86 vs SCE and a λ_{max} of 463 nm.[11] Despite the similar E^*_{red}, in a polymerization with **2a** as the

initiator, only trace amounts of polymer were detected by ^{1}H NMR spectroscopy (Table 5.2, entry 1). Additionally, a significant solution color change was observed, from red to brown (Figure S5.1), likely indicative of decomposition of **PC2**. No significant color change was observed in a reaction with **3** instead of **2a** (Table 5.2, entry 2), suggesting that the enol ether may be reacting deleteriously with **PC2** in some way. Notably, triflate salts have previously been shown to "foul" MF-ROMP reactions (Sean Gitter, unpublished work), and so the **PC2** counterion may be the source of the issue.

The lack of detectable polymer when **3** was used as an initiator was puzzling. Though this exact thioxanthylium had not been used in the original cyclobutanation work, it was confirmed that a cycloaddition with styrene was operative with PC2 (Table 5.2, entry 3). However, when similar conditions were used with norborene instead of styrene, no cyclobutane or ring-opened products were observed (Table 5.2, entry 4). Indeed, only starting materials were detected by ^{1}H NMR spectroscopy. This suggested to us that steric hindrance may be preventing productive interactions between radical cation **3** and **M1**. When moderately elevated temperatures did not resolve this issue (Table 5.2, entry 5), we propsed that the anethole radical cation may be too stable to interact with norbornene. Compared to enol ethers, which have $E_{p/2}$ values ranging from 1.3 to 1.4 V vs SCE, the $E_{p/2}$ of anethole is 1.23 vs SCE. Future work in this area may seek to use aromatic alkenes with higher $E_{p/2}$ values, suggesting more reactive radical cations, to overcome this barrier to success.

Despite this initial inability to expand the class of initiators and photoredox catalysts in MF-ROMP, opportunities for discovery in this area remain. The literature on photoredox catalysis is expansive already and ever-growing. While cursory investigations of other PC classes have not

been immediately successful (see Supplemental Information for details), many still remain to be studied. Expanding both of these scopes has the potential to reveal much about the characteristics of MF-ROMP, and may lead to a more robust polymerization with fewer limitations. One of these current limitations is functional group tolerance, though there is currently promise in a post-polymerization strategy that may circumvent this issue (Sean Gitter, ongoing work). Work should also be done to determine how much changes in setup, which can be very important in photochemical reactions, affect the outcome of the reaction (e.g., light intensity, vial size, headspace). This may help elucidate some of the mechanistic nuances that are currently unclear, such as the role of oxygen in the polymerization.

In conclusion, while there are many possible areas for continued investigation, I believe that we continue to learn more about this polymerization each time we use it, most especially when it does not behave the way we expect it to. As with any scientific endeavor, the key to gaining more control over the system is well-designed experiments, careful data collection, and thoughtful analysis of results. Being vigilant while summarizing experimental outcomes often leads to unexpected places. In fact, it was during photocatalyst screens that I stumbled across solvent effects that eventually culminated in the work summarized in Chapter 4. Whether or not this polymerization is ever considered commercially successful, I believe that it has the foundations to be an excellent educational tool that will teach any graduate student willing to learn both the challenges and triumphs of research. This is a core function of graduate school, and I hope that MF-ROMP will continue to be used to grow novice scientists, helping them learn as it has helped me.

Experimental Procedures & Supplemental Information
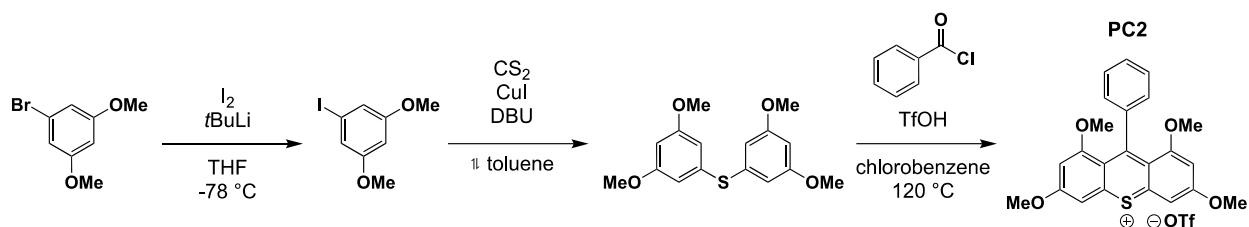
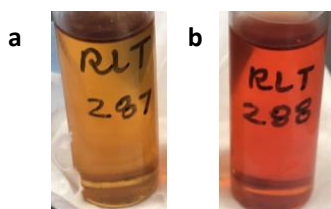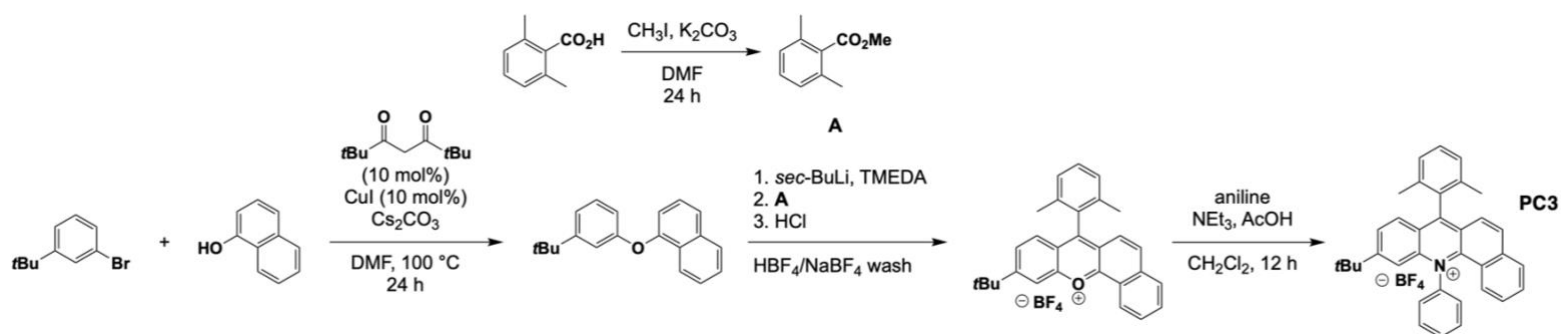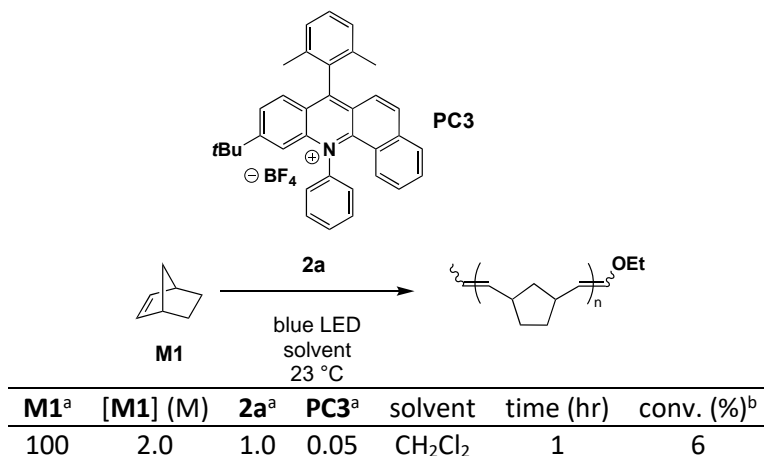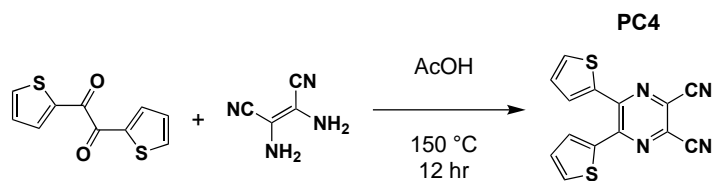**PC2** was synthesized according to literature precedent.[11]

Figure S5.1. Solution color after irradiation for Table 5.2 a) entry 1 and b) entry 2.

**PC3** was synthesized according to literature precedent.[12]

M1[a]	[M1] (M)	2a[a]	PC3[a]	solvent	time (hr)	conv. (%)[b]
100	2.0	1.0	0.05	CH_2Cl_2	1	6

[a]Molar equivalents. [b]Determined by ^{1}H NMR spectroscopy. E^*_{red} = 2.06 vs SCE in MeCN; λ_{max} = 462 nm in DCE. Low conversion is consistent with behavior of pyryliums with higher E^*_{red}.[10]

PC4 was synthesized according to literature precedent.[13] **PC5** is commercially available.
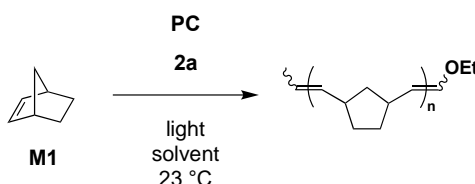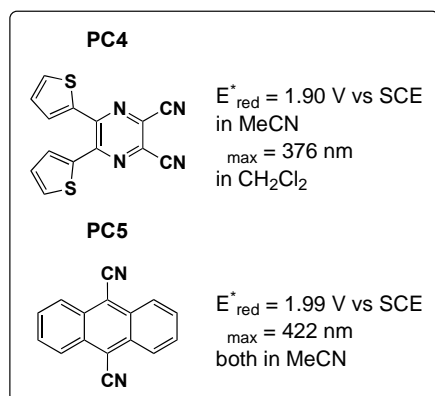
entry	**M1**[a]	[**M1**] (M)	**2a**[a]	HFIP[a‡]	PC (equiv.)	solvent	light	time (hr)	conv. (%)
1	100	2.0	1.0	-	**PC4** (0.2)	CH_2Cl_2	370 nm Kessil	1	n.d.
2	100	2.0	1.0	10	**PC4** (0.2)	CH_2Cl_2	370 nm Kessil	1	n.d.
3	100	2.0	1.0	-	**PC5** (0.2)	CH_2Cl_2	blue LED	19	n.d.
4	100	2.0	1.0	10	**PC5** (0.2)	CH_2Cl_2	blue LED	19	n.d.
5	100	2.0	1.0	10	**PC5** (0.2)	MeCN	blue LED	18	n.d.

[a]Molar equivalents. [b]Determined by ^1H NMR spectroscopy. ‡Cyanoarenes were selected because, as neutral PCs, we hoped that they could facilitate polymerization in bulk (see inset); HFIP was added because we thought the lack of counterion was preventing the radical cation from forming or destabilizing it, and HFIP has been shown to stabilize radical cations (see Chapter 4).

References

1.   Romero, N. A.; Nicewicz, D. A., Organic Photoredox Catalysis. *Chem. Rev.* **2016,** *116*, 10075-10166.

2.   Reckenthäler, M.; Griesbeck, A. G., Photoredox Catalysis for Organic Syntheses. *Adv. Synth. Catal.* **2013,** *355*, 2727-2744.

3.   Wu, C.; Corrigan, N.; Lim, C.-H.; Miyake, G.; Boyer, C., Rational Design of Photocatalysts for Controlled Polymerization: Effect of Structures on Photocatalytic Activities. *Chem. Rev.* **2022,** *122*, 5476-5518.

4.   Ischay, M. A.; Lu, Z.; Yoon, T. P., [2+2] Cycloadditions by Oxidative Visible Light Photocatalysis. *J. Am. Chem. Soc.* **2010,** *132*, 8572-8574.

5.   Riener, M.; Nicewicz, D. A., Synthesis of cyclobutane lignans via an organic single electron oxidant-electron relay system. *Chem. Sci.* **2013,** *4*, 2625-2629.

6.   Tanaka, K.; Iwama, Y.; Kishimoto, M.; Ohtsuka, N.; Hoshino, Y.; Honda, K., Redox Potential Controlled Selective Oxidation of Styrenes for Regio- and Stereoselective Crossed Intermolecular [2 + 2] Cycloaddition *via* Organophotoredox Catalysis. *Org. Lett.* **2020,** *22*, 5207-5211.

7.   Lin, S.; Ischay, M. A.; Fry, C. G.; Yoon, T. P., Radical Cation Diels—Alder Cycloadditions by Visible Light Photocatalysis. *J. Am. Chem. Soc.* **2011,** *133*, 19350-19353.

8.   Tanaka, K.; Asada, Y.; Hoshino, Y.; Honda, K., Visible-light-induced [4 + 2] cycloaddition of pentafulvenes by organic photoredox catalysis. *Org. Biomol. Chem.* **2020,** *18*, 8074-8078.

9.   Tanaka, K.; Asada, Y.; Hoshino, Y., A new cycloaddition profile for *ortho*-quinone methides: photoredox-catalyzed   [6+4]   cycloadditions   for   synthesis   of benzo[*b*]cyclopenta[*e*]oxepines. *Chem. Commun.* **2022,** *58*, 2476-2479.

10.   Pascual, L. M. M.; Dunford, D. G.; Goetz, A. E.; Ogawa, K. A.; Boydston, A. J., Comparison of Pyrylium and Thiopyrylium Photooxidants in Metal-Free Ring-Opening Metathesis Polymerization. *Synlett* **2016,** *27*, 759-762.

11.   Tanaka, K.; Kishimoto, M.; Sukekawa, M.; Hoshino, Y.; Honda, K., Green-light-driven thioxanthylium-based organophotoredox catalysis: Organophotoredox promoted radical cation Diels-Alder reaction. *Tetrahedron Lett.* **2018,** *59*, 3361-3364.

12.   White, A.; Wang, L.; Nicewicz, D., Synthesis and Characterization of Acridinium Dyes for Photoredox Catalysis. *Synlett* **2019,** *30*, 827-832.

13.   Zhao, Y.; Zhang, C.; Chin, K. F.; Pytela, O.; Wei, G.; Liu, H.; Bures, F.; Jiang, Z., Dicyanopyrazine-derived push–pull chromophores for highly efficient photoredox catalysis. *RSC Adv.* **2014,** *4*, 30062-30067.